



Bayesian time-frequency analysis of the vehicle–bridge dynamic interaction effect on simple-supported resonant railway bridges



Kodai Matsuoka ^{a,*}, Kiyoyuki Kaito ^b, Masamichi Sogabe ^c

^a Railway Technical Research Institute Railway Dynamics Division 2-8-38, Hikari-cho, Kokubunji-shi Tokyo 185-8540, Japan

^b Osaka University Graduate School of Engineering, Division of Global Architecture, 2-1 Yamada-oka, Suita, Osaka 565-0871, Japan

^c Railway Technical Research Institute Administration Division 2-8-38, Hikari-cho, Kokubunji-shi Tokyo 185-8540, Japan

ARTICLE INFO

Article history:

Received 13 September 2018

Received in revised form 10 September 2019

Accepted 13 September 2019

Available online 24 September 2019

Keywords:

Vehicle–bridge interaction

Resonance

Bayesian estimation

MCMC

TVARX

ABSTRACT

Monitoring the conditions or damages of bridges under train passages demands a high-accuracy modal-characteristic identification method that separates the apparent fluctuations caused by vehicle–bridge dynamic interaction (VBI) effects from other fluctuations. This study proposes a novel method based on a time-varying autoregressive model, which is solved using a hierarchical Bayesian estimation approach. The VBI effect is estimated from the displacement response of the railway bridges as temporal fluctuations of the natural frequency and modal damping ratio. The exogenous variable is the train load, expressed as an external force. Numerical experiments verified the higher accuracy of the proposed method than the existing method. The influences of train speed and rail irregularity on the VBI effects are clarified by the application of the proposed method to various VBI simulations. The proposed method was applied to the measured resonance responses of actual bridges and succeeded in empirically demonstrating the decreased natural frequency and the increased modal damping ratio under train passage. Additionally, using the proposed method, modal characteristics variation due to VBI effect calculated using VBI model simulation was verified by comparing with those estimated from the measured results.

© 2019 The Author(s). Published by Elsevier Ltd. This is an open access article under the CC BY-NC-ND license (<http://creativecommons.org/licenses/by-nc-nd/4.0/>).

1. Introduction

A vehicle–bridge interaction (VBI) is a dynamic interaction between a railway bridge and a passing train. In real world [1], VBI is a time-varying vibration system problem; a vehicle passing via a railway bridge acts as an additional mass on the bridge. Because the damping of a vehicle is sufficiently larger than that of a bridge, it acts as an additional damping that absorbs and reduces the bridge vibration [1–4].

From the practical viewpoint, VBI should be understood to evaluate the resonance phenomena in the design of high-speed railway bridges. Particularly, understanding the VBI effect on resonance was important for evaluating the dynamic response amplification owing to the resonance of bridges and high-speed railways at speeds of more than 200 km/h [3–6]. Various

Abbreviations: DK, Durbin and Koopman; MCMC, Markov chain Monte Carlo; ML, Moving loads; PDF, Probability density function.

* Corresponding author at: Structural Mechanics in Railway Dynamics Division, 2-8-38, Hikari-cho, Kokubunji-shi Tokyo 185-8540, Japan.

E-mail addresses: matsuoka.kodai.13@rtri.or.jp (K. Matsuoka), kaito@civil.eng.osaka-u.ac.jp (K. Kaito), sogabe.masamichi.78@rtri.or.jp (M. Sogabe).

simulations on the VBI effect has been clarified, revealing that VBI can offer an additional damping effect (apparent increase in the damping ratio) and additional mass effect (apparent decrease in natural frequency) on the railway bridge resonance [3,7–10]. However, bridges can be conservatively designed without considering the complex VBI effects. Thus, limited attention has been given to temporal variations of the natural frequency and modal damping ratio because VBI may occur on a railway bridge when a train passes, except in special cases [11].

However, elucidating and quantifying the time-varying behaviors of the VBI effect is more important for the efficient maintenance and management of railway bridges owing to its structural health monitoring that has been urgently researched in recent years [12–14]. When a train passes over a bridge, the modal characteristics related to structural performance, such as the natural frequency of the bridge, are identified from the bridge responses measured by installed sensors. Abnormalities and damages are detected from the temporal changes in the responses [12]. As the natural frequency of a railway bridge is often insensitive to deteriorations or damages [13,14], identification of the modal characteristics from the traffic response requires a highly accurate method [11,15]. However, the estimation accuracy is reduced by the VBI effect. The displacement responses of the VBI and moving load (ML) models are compared in Fig. 1. The passing vehicles in ML models are modeled as non-vibrating concentrated constant moving loads. However, the two responses are clearly mismatched, confirming that the VBI effect alters the bridge response. The difference between the two models reflects the estimation error, and the original damage and deterioration information of the railway bridge (which one desires to know) is obscured. When quantifying the VBI response to train passage, one must estimate the apparent variation of the modal characteristics of the railway bridge caused by the VBI. These variations are expressed as equivalent and time-varying additional modal parameters (Fig. 2) [1,4]. The analytical methods for time-varying dynamic systems are one of the new tools to quantify the VBI effects based on the measured data [16].

In recent years, the theory and technology of the time-varying dynamics systems have rapidly developed. The data-based systems and parameter estimation problems are called identification/inverse problems. Further, methods for identifying the time-varying systems are classified in [16] and [17], by comparing their features and performances. A study [17] reveals that the identification of time-varying systems, classified into the time–frequency method category, are classified as nonparametric or parametric methods. Majority of the identification methods in the frequency domain, such as short-time Fourier transforms [18,19], Cohen classes [20–22], wavelet-based methods [23–26], and Hilbert–Huang transform [27,28], are characterized as nonparametric approaches. However, the time domain methods [17,29,30] based on the time-dependent state space and time-dependent autoregressive moving average (TARMA) models are categorized as parametric approaches. Particularly, the TARMA-based methodology has significantly developed in recent years [17]. The time domain parametric approaches are classified into unstructured evolution (UPE), stochastic parameter evolution (SPE), and deterministic parameter evolution (DPE) because of the differences in modeling of the time-dependent coefficients [17]. Spiridonakos and Fassioish [30] compared and verified the accuracy and limitations of these parametric time domain methods by applying a moving mass added beam experimental approach.

However, the application of time-varying system identification techniques to real structures, such as structural health monitoring (SHM), is still an important and novel challenge, as revealed by Garibaldi and Fassioish [16]. In particular, few cases of the bridge response application are noted, largely affected by the actual vehicle with complex vibration systems that travel on rail with irregularities. Cantero et al. [26] and Ülker-Kaustell and Karoumi [31] applied wavelet transforms to the

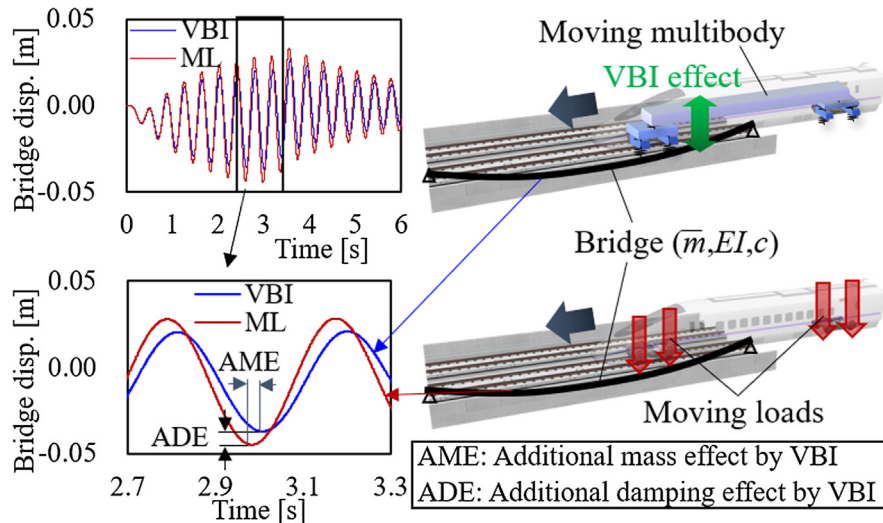


Fig. 1. Comparison of displacement responses during a train passage, calculated by the VBI and ML models (Span length, 25 m; bridge frequency, 2.7 Hz; modal damping ratio, 2%; train speed, 230 km/h).

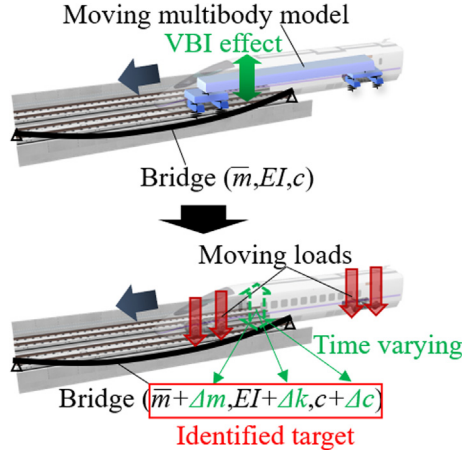


Fig. 2. Concept of VBI effect evaluated in this study: The VBI effect is evaluated through (time-varying) equivalent additional parameters of the bridge.

acceleration responses of a railway bridge when trains were passing. Their results clarified that the dominant vibration frequency changes between during and after traveling train, and that the excitation force of the traveling train becomes dominant in the time-frequency domain of the bridge response during the passing of the trains. Matsuoka et al. applied a time-varying vector AR (TV-VAR) model to the acceleration responses when the train passed at low speeds and identified the behavior of natural frequency reduction in a short time corresponding to the passage of each wheelset [32]. These applications employ only the output for performing time-frequency analysis. Therefore, it cannot be denied that the time-varying bridge modal characteristics by the VBI may not be separated from the excitation characteristics of the passing train including regular axle arrangements and rail irregularities.

The VBI effect is the most pronounced (i.e., the largest error in the identification of the linear system) in the resonance state in which the excitation frequency of the traveling train and the natural frequency of the bridge coincide [3,8,9]. This state is classified as forced vibration on the existing method [26]. The aforementioned, output only identification methods that does not consider the external force characteristics are unable to separate the input from the vehicle and the bridge modal characteristics of the bridge (and the VBI effect mixed there) from the resonant bridge [32,33]. In addition, the speed of high-speed railway that can cause resonance exceeds 200 km/h. It means that the period available for identification is only a very short [34]. Comparing between parametric and non-parametric methods, parametric methods such as AR models have an advantage to be able to satisfy the requirement for high temporal resolution [35,36]. This study provides a methodology to identify the time-varying modal characteristics using the VBI effect of the measured time-history bridge response when a train passes. This study focuses on bridge resonance when the VBI effect is the most pronounced. Specifically, the VBI-induced time varying bridge modal characteristics and the traveling train excitation hidden in the measurement response of the resonant bridges is separated by developing a time-varying autoregressive with exogenous variable (TVarX) model. The effect of the moving loads which is the input provided from the traveling train to the bridge is considered to be an exogenous variable in TVarX model. Proposed TVarX model may not be able to completely explain the unsteady and complex dynamics of the bridge when the train passes [37]. However, the proposed method overcoming the difficulties of time-frequency analysis for time-varying modal characteristics can provide novel information related to the VBI effect that was not obtained from the high-speed railway bridge resonance conditions so far.

The proposed TVarX model is classified as SPE [16,17,30]. SPE introduces stochastic smoothness constraints [33,35]. It is advantageous to reflect partial and vague prior information such as "it will change gradually (continuously) with the passing of each wheelset but we do not know when or how." Thus, SPE can avoid the bias caused by excessive constraints (structuring) in this study. When compared with DPE, SPE has a large computational cost for estimating many unknown parameters [17,30]. In addition, the estimation process becomes complicated owing to the hierarchical parameters [38]. However, the framework of the hierarchical Bayesian methods based on the Bayesian theory and MCMC method made the batch estimation of all the large number of hierarchical parameters possible [39,40]. These developments are applied in the econometric field [41–45]. This research evaluates the VBI effect using the TVarX model in the hierarchical Bayesian framework. For efficient parameter estimation, the following two approaches that are unique to this research are introduced. One is simplification using modal reduction (reduction of the degree of freedom) of the resonant bridge dynamics model during the passage of trains. Generally, the vibrations of the high-speed railway bridges are expressed in several low-order modes [1,4,9]. In addition, the fundamental vibration mode of the bridge is dominant during resonance, which is the target of this research [3,5]. By limiting the analysis to a fundamental vibrational model, the model parameters are estimated. Another is the efficient estimation approach of the time-variant coefficients using MCMC calculation. Durbin and Koopman [43] have succeeded in reducing the computational complexity of the huge filter/smoothing calculation process by employing the independence of variance in conditional probability (Appendix IV) [46]. Despite the efficiency of the Durbin and Koopman

[43], the authors could not find any applications in the vibration engineering field. This study reduces the enormous calculation cost required for time-varying coefficient estimation by incorporating this advanced method into the hierarchical Bayesian estimation of the TVARX model.

Through the application of the proposed method to numerical experiments and VBI simulations, this study clarifies the estimation accuracy of the temporal variation of modal characteristics and the effects of various factors. And then, the proposed method is applied to the measurement data of the real-world resonant bridges for analyzing the VBI effects in the actual bridges.

First, the basic performances, such as the effect of introducing exogenous variables and the effect of added noise, are verified using numerical experiments using the TVARX model as a waveform generation and estimation model. However, the dynamic response and VBI effects of the resonant bridge during the passage of a train are influenced not only by the moving loads on the traveling vehicle, but also the train speed, track irregularities, bridge type and spatial/temporal bridge parameter variation such as bridge cracks. [1,4,9,37,48,49]. Using VBI model simulations, we verify the effects of train speed and track irregularities on the estimation results obtained using the proposed method. The bridge type was assumed to be a simple girder type, which is extensively observed in Japanese high-speed railway [4]. However, the assumption of modal reduction (representation of dynamics in one degree of freedom), introduced in the proposed method, does not hold for continuous beam bridges [47]. Therefore, the application of continuous beam bridges is not covered in this study. In addition, the effects of the crack opening and closing that occurred on the bridge were not considered [49]. Many theoretical and experimental researches on crack indicated the natural frequency changes depending on the bridge amplitude [50–52]. In addition, many methods for estimating the crack position and degree have been proposed and verified using the numerical and laboratory experiments [53–56]. However, in case of cracked bridges, it is not currently easy to determine whether the time variation of the mode characteristics observed in the estimation results of the actual measurement data is the effect of VBI or breathing crack [16]. Therefore, only the VBI effect is considered in this study. The combined effects of breathing crack and VBI [16] and its evaluation will be discussed in other literature following this study.

Finally, the proposed method is applied to the measured displacement responses at the resonance simple-supported bridges in Japanese high-speed railway to analyze the VBI effect in a real-world situation. In the application of the actual measured displacement response, the influence of the aforementioned factors was suppressed to estimate the VBI effect under resonance situation. Data were measured during the test run before opening the bridges in which the crack was not confirmed through the inspections. Therefore, it can be assumed that the effect of the crack is not present or negligible in the target bridges. Similarly, running tests are conducted in a good track condition (total amplitude of less than 5 mm for 3–50-m wavelength [57]) for track maintenance. Therefore, the effects of rail irregularities are also suppressed. In addition to the selection of applicable bridges specialized for the VBI effect analysis, the proposed method is also applied to VBI simulation [37] that reproduces the target bridge responses to verify the spatial and temporal parameter variations and track irregularities. The VBI effect is also estimated from the displacement responses simulated by the VBI model without considering the rail irregularities and cracks. The comparison with the estimation result based on the actual measured responses verifies the assumption of the application with the actual measurement data. In the real environment, the VBI effect estimated by the proposed method using the measured data, where various factors are eliminated, is important evidence for the elucidation of the VBI effect and the examination of the simple modeling of VBI effect in the future.

2. Formulation of the hierarchical Bayesian TVARX model

2.1. Equation of motion of a beam during train passage

Many symbols are presented in this study to describe the physical model, statistical model, and estimation process using uniform mathematical formulas. The symbols used in this study are summarized in [Appendix I](#). Although derived in previous studies (e.g., [4,9,37]), Eqs. (1)–(8) are important for modeling the VBI effect, so their preconditions and physical interpretations are briefly stated here.

[Fig. 3](#) schematizes the target VBI model. The bridge is modeled as a simple-supported beam with a uniform cross-section along the rail direction. In [Fig. 3](#), a train with n_w wheelsets travels from left to right at velocity v along a bridge with span length L . A vehicle model has six degrees of freedom for car body vertical displacement $z_{c,t}$, pitching rotation $\psi_{c,t}$, front/rear bogie vertical displacement $z_{t1,t}/z_{t2,t}$, and pitching rotation $\psi_{t1,t}/\psi_{t2,t}$. The symbols m_c (m_t) and J_c (J_t) in [Fig. 3](#) denote the mass and rotational inertia, respectively, of the vehicle body (bogie). m_w is the mass of the wheelset. c_s (c_p) and k_s (k_p) are the viscous damping and spring coefficients, respectively, of the secondary (primary) suspensions. k_{cs} and c_{cs} are the viscous damping and spring coefficients, respectively, of the car body connectors, and b , r , and L_v are the distances between the wheelsets on a bogie, the bogie centers on a vehicle, and the vehicle length, respectively. A rigid contact was assumed between the wheel and the rail.

Assuming a Bernoulli Euler beam, an arbitrary point vertical response $y_{x,t}$ can be obtained on the bridge. This can be given as

$$\bar{m} \frac{\partial^2 y_{x,t}}{\partial t^2} + c \frac{\partial y_{x,t}}{\partial t} + EI \frac{\partial^4 y_{x,t}}{\partial x^4} = \sum_{i=1}^{n_w} P_s \delta(x - vt - \tau_i) + \sum_{i=1}^{n_w} P_d \delta(x - vt - \tau_i), \quad (1)$$

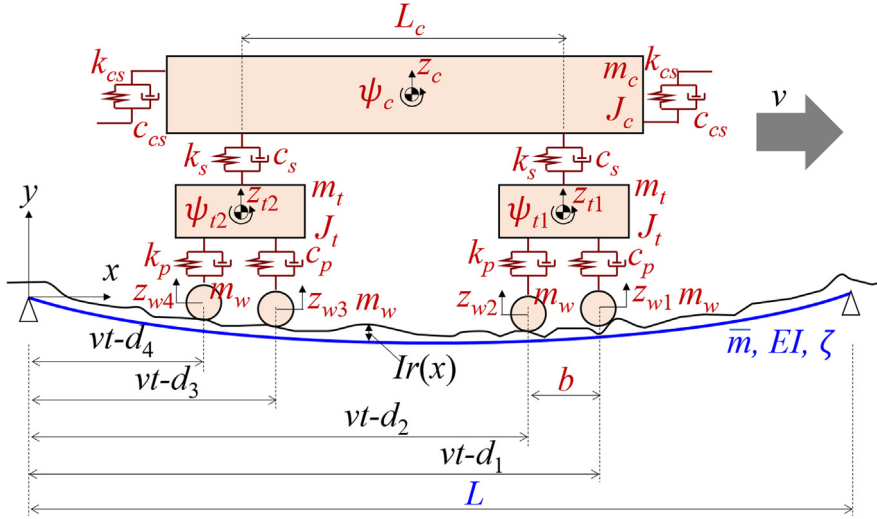


Fig. 3. Passage of a 6 degree-of-freedom vehicle model on a simple-supported beam.

$$\sum_{i=1}^{nw} P_d \delta(x - vt - \tau_i) = - \sum_{i=1}^{nw} m_w \frac{\partial^2 (y_{x-vt-\tau_i,t})}{\partial t^2} + \sum_{i=1}^{nw} c_p \frac{\partial (z_{ti,t} - y_{x-vt-\tau_i,t})}{\partial t} + \sum_{i=1}^{nw} k_p (z_{ti,t} - y_{x-vt-\tau_i,t}) - \sum_{i=1}^{nw} m_w \times \frac{\partial^2 Ir(x-vt-\tau_i)}{\partial x^2} - \sum_{i=1}^{nw} c_p \frac{\partial Ir(x-vt-\tau_i)}{\partial x} - \sum_{i=1}^{nw} k_p Ir(x-vt-\tau_i) \quad (2)$$

where \bar{m} , c , and EI are the unit-length mass, damping coefficient, and bending stiffness of the bridge, respectively, δ is the Dirac delta function, τ_i is the distance from the left end of the beam to the i th wheelset at the initial time point. $z_{ti,t}$ denotes the bogie vertical displacement at a position above the i th wheelset. $Ir(x)$ is the rail irregularity. $P_{i,D}$ is the dynamically time-varying component in the wheel load, and $P_{i,S}$ is the stationary wheel load. The equations of motion for the vehicle are provided in [Appendix II](#).

The coordinate system is converted to the modal coordinate system using modal shape vector $\Phi_{n,x}$ and modal displacement $z_{n,t}$ in which $n (n = 1, \dots, N)$ is the modal number as follows:

$$y_{x,t} = \sum_{n=1}^N z_{n,t} \Phi_{n,x} = \sum_{n=1}^N z_{n,t} \sin \frac{n\pi x}{L} \quad (3)$$

The primary deflection mode $n = 1$ (the main displacement response component at mid-span) is given by

$$m_b \ddot{z}_{1,t} + c_b \dot{z}_{1,t} + k_b z_{1,t} = \sum_{i=1}^{nw} A_{i,t} P_{i,S} + \sum_{i=1}^{nw} A_{i,t} P_{i,D} \quad (4)$$

$$A_{i,t} = \sin \left\{ \frac{\pi(vt - \tau_i)}{L} \right\} \left\{ H\left(t - \frac{\tau_i}{v}\right) - H\left(t - \frac{\tau_i + L}{v}\right) \right\} \quad (5)$$

$$m_b = \frac{\bar{m}L}{2}, c_b = \frac{cL}{2}, k_b = \frac{\pi^4 EI}{2L^3} \quad (6)$$

Here, H is the Heaviside unit function. $A_{i,t}$ is a modal function of the bridge, and $\sum_{i=1}^{nw} A_{i,t}$ is the modal excitation force. m_b , c_b , and k_b are the modal mass, damping, and stiffness coefficients of the bridge. In this study, $n = 1$, so $z_{1,t}$ is simply described as z_t . The natural frequency f and modal damping ratio ξ are expressed as follows:

$$f = \frac{1}{2\pi} \sqrt{\frac{k_b}{m_b}} \quad (7)$$

$$\xi = \frac{c_b}{2\sqrt{m_b k_b}} \quad (8)$$

2.2. Derivation of the ARX model from the ML model

This subsection shows that the equations in the ARX model are not merely statistical expressions, but are equivalent to the motions of the ML model. When the dynamic component of the wheel load $P_{i,D}$ is set to 0, the ML model reduces to

$$m_b \ddot{z}_t + c_b \dot{z}_t + k_b z_t = \sum_{i=1}^{nw} A_{i,t} P_{i,S} \quad (9)$$

By the central difference concept [38] at equal intervals Δ , Eq. (8) can be differentiated and discretized as follows:

$$\left(\frac{m_b}{\Delta^2} + \frac{c_b}{2\Delta} \right) z_{t+\Delta} = \sum_{i=1}^{nw} A_{i,t} P_{i,S} - \left(k_b - \frac{2m_b}{\Delta^2} \right) z_t - \left(\frac{m_b}{\Delta^2} + \frac{c_b}{2\Delta} \right) z_{t-\Delta} \quad (10)$$

Introducing the discrete time points $m (m = 1, \dots, M)$, which are related to continuous time as $t = (m-1)\Delta$, and adding an observation noise ϵ_m , the following ARX model is obtained:

$$z_m = \mathbf{A}_m \boldsymbol{\alpha} + \mathbf{Z}_m \boldsymbol{\beta} + \epsilon_m \quad (11)$$

where

$$\mathbf{A}_m = [A_{1,m-1}, \dots, A_{nw,m-1}] \quad (12a)$$

$$\boldsymbol{\alpha} = [\boldsymbol{\alpha}_1, \dots, \boldsymbol{\alpha}_{nw}]^T, \quad (12b)$$

$$\mathbf{Z}_m = [z_{m-1}, z_{m-2}], \quad (12c)$$

$$\boldsymbol{\beta} = [\beta_1, \beta_2]^T \quad (12d)$$

$$\epsilon_m \sim N(0, \sigma_\epsilon^2) \quad (12e)$$

$$\beta_1 = -\frac{k_b - 2m_b/\Delta^2}{\gamma}, \quad \beta_2 = -\frac{m_b/\Delta^2 - c_b/2\Delta}{\gamma} \quad (12f)$$

$$\gamma = \frac{m_b}{\Delta^2} + \frac{c_b}{2\Delta} \quad (12g)$$

$$\boldsymbol{\alpha}_i = P_{i,S}/\gamma \quad (12h)$$

T on the right shoulder represents the transposition operation of the vector and matrices. \mathbf{A}_m is the vector that includes the bridge modal function corresponding to each wheelset calculated in Eq. (5), and $\boldsymbol{\alpha}$ is the unknown vector expressing the regression coefficient of modal function, which controls the magnitude of the excitation force. $\boldsymbol{\beta}$ is an unknown autocorrelation coefficient vector. The observation noise ϵ_m is the normal distribution $N(0, \sigma_\epsilon^2)$ with an average value of 0 and variance σ_ϵ^2 .

Fig. 4 compares the bridge responses during train passage calculated using the ML and ARX models. The bridge had a span length of 30 m, a natural frequency of 2.7 Hz, a modal damping ratio of 0.02, and a unit-length mass of 22 t/m. The train consisted of eight vehicles, each of length 25 m, a bogie center distance of 17.5 m, a wheelset distance of 2.5 m, wheel loads of 135 kN, time interval Δ of 0.001 s, and a passing speed of 220 km/h. ϵ_m of the ARX model was set to 0. The results of both models are consistent, indicating that both models express the same physical phenomena, including resonance.

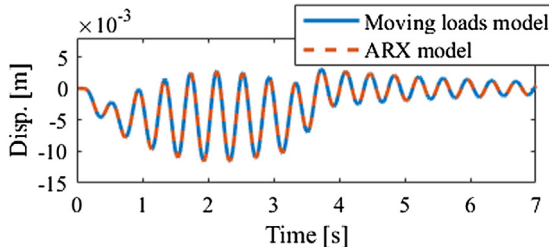


Fig. 4. Comparison of displacement responses calculated by Moving Load model and ARX model.

2.3. Derivation of the TVARX model from the VBI model

This subsection relates the VBI model to the TVARX model, which allows temporal variation in the parameters of the ARX model. The VBI effect influences the modal characteristics of the bridge by coupling the bridge with the vehicle.

Substituting Eq. (2) into Eq. (4) gives

$$\begin{aligned} & \left(m_b + \sum_{i=1}^{nw} A_{i,t}^2 m_w \right) \ddot{z}_t + \left(c_b + \sum_{i=1}^{nw} A_{i,t}^2 c_p \right) \dot{z}_t + \left(k_b + \sum_{i=1}^{nw} A_{i,t}^2 k_p \right) z_t \\ & = \sum_{i=1}^{nw} A_{i,t} P_{i,S} + \sum_{i=1}^{nw} A_{i,t} \left(c_p \dot{z}_{ti,t} + k_p z_{ti,t} - m_w \frac{\partial^2 Ir(x - vt - \tau_i)}{\partial x^2} - c_p \frac{\partial Ir(x - vt - \tau_i)}{\partial x} - k_p Ir(x - vt - \tau_i) \right) \end{aligned} \quad (13)$$

Eq. (13) shows that bridges with a passing train are time-variant systems because of the time variant coefficient $A_{i,t}$ on the left side of Eq. (13). The problem is the second term on the right side in which the terms are related to bogie displacement, velocity, and track irregularities. If a part corresponds to the bridge displacement, velocity, and acceleration, the corresponding part can be shifted to the left side. Thus, they generate a part of the VBI effect. The actual bogies and car bodies vibrate depend on the rail irregularity and bridge displacement. Therefore, it is undeniable that some part of these vibrations contributes to the VBI effect. Because it is not possible to simply understand the dependency of vehicle vibration on the bridge vibration, the VBI effect has been studied by simulation using VBI models. Thus, this research estimates this parameter using the TVARX model. This study assumed that Eq. (13) can be represented by Eq. (14).

$$\left(m_b + \sum_{i=1}^{nw} A_{i,t}^2 \Delta m_v \right) \ddot{z}_t + \left(c_b + \sum_{i=1}^{nw} A_{i,t}^2 \Delta c_v \right) \dot{z}_t + \left(k_b + \sum_{i=1}^{nw} A_{i,t}^2 \Delta k_v \right) z_t = \sum_{i=1}^{nw} A_{i,t} P_{i,S} + \sum_{i=1}^{nw} A_{i,t} \hat{P}_{i,D} \quad (14)$$

where Δm_v , Δc_v , and Δk_v are the additional components of the vehicle mass, damping, and stiffness to the bridge modal mass, damping, and stiffness resulting from the vehicle response and rail irregularities associated with the bridge response, respectively. Also, $\sum_{i=1}^{nw} A_{i,t} \hat{P}_{i,D}$ is a component obtained by subtracting the vehicle response components related to the bridge

responses from the second term on the right side of the Eq. (13). With the assumption about $\sum_{i=1}^{nw} A_{i,t} \hat{P}_{i,D}$, the natural frequency f_t and the modal damping ratio ξ_t , which includes the variation of the modal characteristics of the railway bridge due to the VBI effect on the time-history response during the train passage, is expressed as follows:

$$f_t = \left(1 - \frac{\kappa_t^m}{2} \right) \left(1 + \frac{\kappa_t^k}{2} \right) f \quad (15)$$

$$\xi_t = \left(1 + \kappa_t^c \right) \left(1 - \frac{\kappa_t^m}{2} \right) \left(1 - \frac{\kappa_t^k}{2} \right) \xi \quad (16)$$

where κ_t^m , κ_t^c and κ_t^k are the mass, damping, and stiffness ratios between the bridge and some parts of the vehicle corresponding to the VBI.

$$\kappa_t^m = \frac{\sum_{i=1}^{nw} A_{i,t}^2 \Delta m_t}{m_b} \quad (17a)$$

$$\kappa_t^c = \frac{\sum_{i=1}^{nw} A_{i,t}^2 \Delta c_t}{c_b} \quad (17b)$$

$$\kappa_t^k = \frac{\sum_{i=1}^{nw} A_{i,t}^2 \Delta k_t}{k_b} \quad (17c)$$

In deriving Eqs. (15) and (16), we used the approximation $(1 + \kappa)^n \approx 1 + n\kappa$ ($|\kappa| \ll 1$).

Discretizing Eq. (14) by the central difference scheme as in the previous section, the VBI model becomes the ARX model of Eq. (18) with a time-varying coefficient β_m . This model is the TVARX model.

$$z_m = \mathbf{A}_m \alpha + \mathbf{Z}_m \beta_m + \epsilon_m \quad (18)$$

$$\beta_m = [\beta_{1,m}, \beta_{2,m}]^T \quad (19a)$$

$$\beta_{1,m} = - \frac{k_b - 2(1 + \kappa_{m-1}^m)m_b/\Delta^2}{\gamma_m} \quad (19b)$$

$$\beta_{2,m} = -\frac{(1 + \kappa_{m-1}^m)m_b/\Delta^2 - (1 + \kappa_{m-1}^c)c_b/2\Delta}{\gamma_m} \quad (19c)$$

$$\gamma_m = (1 + \kappa_{m-1}^m)\frac{m_b}{\Delta^2} + (1 + \kappa_{m-1}^c)\frac{c_b}{2\Delta} \quad (19d)$$

The component $\sum_{i=1}^{nw} A_{i,t} \hat{P}_{i,D}$ is included in the observation error ϵ_m according to the normal distribution $N(0, \sigma_\epsilon^2)$. The difference of Eq. (18) with respect to Eq. (11) is only β_m , which is a time-varying autocorrelation coefficient vector depending on the time point m . The time-varying coefficient β_m has already been proposed for wavelet functions, polynomial approximation methods, and similar applications [17,38,58]. In the present study, it becomes a function of the superposition $\sum A_{i,t}^2$ of the beam modal shapes given by Eq. (5). However, introducing this function places additional constraints on the model and may lead to a false understanding of the VBI phenomenon. As the VBI effect in the time-history response is poorly understood, the estimation should avoid assumptions on the function as far as possible, and the function should be improved based on the results. Therefore, in the present study, the time-varying coefficient β_m is described by the following random walk process [35,36,43]:

$$\beta_{m+1} = \beta_m + \mathbf{v}_m, (m = 1, \dots, M-1) \quad (20)$$

where

$$\mathbf{v}_m \sim N(0, \Sigma_v) \quad (21a)$$

$$\beta_1 \sim N(\beta_0, \Sigma_\beta) \quad (21b)$$

\mathbf{v}_m and ϵ_m are independent, and β_0 expresses the initial distribution of β_1 . The TVARX model is composed of Eqs. (18) and (20). In a Bayesian modeling sense, β_m can be understood as a hierarchical Bayesian model with a hierarchical prior distribution [43].

By solving the characteristic Eq. (22), the time-varying coefficient β_m at time point m can be converted to the natural frequency f_m and the modal damping ratio ξ_m of the bridge, calculated using Eqs. (23) and (24), respectively. Here, the pole $\lambda = \tilde{\lambda}$ satisfies the characteristic Eq. (22).

$$|\lambda^2 + \lambda\beta_{1,m} + \beta_{2,m}| = 0 \quad (22)$$

$$f_m = \frac{1}{2\pi\Delta} \sqrt{\operatorname{Re}\{\ln(\tilde{\lambda})\}^2 + \operatorname{Im}\{\ln(\tilde{\lambda})\}^2} \quad (23)$$

$$\xi_m = \frac{-\operatorname{Re}\{\ln(\tilde{\lambda})\}^2}{\sqrt{\operatorname{Re}\{\ln(\tilde{\lambda})\}^2 + \operatorname{Im}\{\ln(\tilde{\lambda})\}^2}} \quad (24)$$

where $\operatorname{Re}\{\cdot\}$ and $\operatorname{Im}\{\cdot\}$ represents the extraction operations of the real and imaginary parts of a complex number, respectively.

The natural frequency f_m and modal damping ratio ξ_m of the bridge at each time point m are called the instantaneous natural frequency and the instantaneous modal damping ratio, respectively. In the TVARX model, the instantaneous power spectrum $PS_{f,m}$ at the discrete time point m is calculated using Eq. (25). The phenomena of nonlinear systems or nonstationary systems are often clarified on a frequency-versus-time distribution of the instantaneous power spectrum. This distribution is called an *energy map* [31]. The present study derives the instantaneous power spectrum, the instantaneous natural frequency, and the instantaneous modal damping ratio of the bridge alone (the VBI effect), with the external force characteristics of the traveling train removed. This separation is a noteworthy difference between our instantaneous power spectrum and the energy maps of a previous study [31]. As shown in the Application section, the instantaneous power spectrum with the separated external force characteristics enables detailed analysis of the VBI effect on the bridge, which have not been accomplished thus far.

$$PS_{f,m} = \frac{\sigma_\epsilon^2}{|1 - \beta_{1,m} \exp(-2\pi if) - \beta_{2,m} \exp(-2\pi if)|} (-1/2\Delta \leq f \leq 1/2\Delta) \quad (25)$$

2.4. Hierarchical Bayesian estimation

The TVARX model is known as a time-varying input/output system in machine control [59] and as a time-series analysis method in econometric economy [44]. Estimation methods in machine control are usually based on transfer functions with

filters [60]. On the other hand, econometric economy applications have been implemented by Bayesian estimation and maximum likelihood estimation, and their input components cannot be arbitrarily controlled [35]. The authors proposed a hierarchical Bayesian estimation method called the time-varying vector autoregressive (TVVAR) model, which uses the Gibbs sampling approach (a Markov chain Monte Carlo (MCMC) method) [32]. The hierarchical Bayesian estimation method in the present study is novel in two respects. First, the MCMC incorporates the estimation of exogenous variables. Second, the time-varying coefficient β_m adopts the efficient sampling scheme of multiple conditional probability proposed by Durbin and Koopman [43], which avoids the large computational cost of previous hierarchical Bayesian estimation processes. These adaptations realize fast estimation while considering the uncertainty in the natural frequency and modal damping ratio.

We now briefly describe the general Bayes estimation method (details are given in [39]). Bayesian estimation computes the posterior distribution of unknown parameters based on their prior distribution and a likelihood function defined by the observation data. Here, $\theta = [\beta_1, \dots, \beta_M, \sigma_\epsilon, \Sigma_v, \alpha]$ and $\tilde{\mathbf{z}} = [\tilde{z}_1, \dots, \tilde{z}_M]$ represent the unknown parameter vector of TVARX model and observation data vector of the displacement response during train passage, respectively. The random variable θ is assumed to follow the prior probability density function (PDF) $\pi(\theta)$. When the observation data $\tilde{\mathbf{z}}$ are known, Bayes' theorem predicts the simultaneous posterior PDF $\pi(\theta|\tilde{\mathbf{z}})$ of the unknown parameter vector θ as follows [39]:

$$\pi(\theta|\tilde{\mathbf{z}}) \propto L(\tilde{\mathbf{z}}|\theta)\pi(\theta) \quad (26)$$

The simultaneous posterior PDF $\pi(\theta|\tilde{\mathbf{z}})$ is the updated distribution of the parameters of the TVARX model. The update is based on the observation information. The prior PDF $\pi(\theta)$ for the TVARX model is formulated as

$$\pi(\theta) = \pi(\sigma_\epsilon)\pi(\alpha)\pi(\Sigma_v) \sum_{m=0}^{M-1} \pi(\beta_{m+1}|\beta_m, \Sigma_v) \quad (27)$$

Owing to the hierarchy of prior PDFs, such as β_m and β_{m+1} or β_m and Σ_v , Eq. (27) is called a hierarchical Bayesian model. Such a model can be estimated collectively while explicitly considering the dependency between parameters, as described below.

2.5. Likelihood and prior PDF

To formulate the posterior PDF, one requires the likelihood function and the prior PDF. We first define the likelihood function. Under the condition of the unknown parameter θ with certain values $\bar{\theta} = [\bar{\beta}_1, \dots, \bar{\beta}_M, \bar{\sigma}_\epsilon, \bar{\Sigma}_v, \bar{\alpha}]$, the likelihood $L(\tilde{\mathbf{z}}|\bar{\theta})$ is expressed as

$$L(\tilde{\mathbf{z}}|\bar{\theta}) = \frac{1}{2\pi\sqrt{\bar{\sigma}_\epsilon^2}} \prod_{m=1}^M \exp \left\{ -\frac{(\tilde{z}_m - \bar{z}_m)^2}{2\bar{\sigma}_\epsilon^2} \right\} \quad (28)$$

where

$$\bar{z}_m = \mathbf{A}_m \bar{\alpha} + \mathbf{Z}_m \bar{\beta}_m \quad (29)$$

Because the prior PDF is hierarchical, $\mathbf{B} = [\beta_1, \dots, \beta_M]$ in terms of Σ_v is equivalent to the observed information in general Bayesian estimation. Therefore, when the matrix $\bar{\Sigma}_v$ is known, the occurrence probability $L(\mathbf{B}|\bar{\Sigma}_v)$ is expressed in the form of a likelihood as follows:

$$L(\mathbf{B}|\bar{\Sigma}_v) = \frac{1}{2\pi\sqrt{|\bar{\Sigma}_v|}} \cdot \prod_{m=1}^{M-1} \exp \left\{ -\frac{1}{2} (\beta_{m+1} - \beta_m)^T \bar{\Sigma}_v^{-1} (\beta_{m+1} - \beta_m) \right\} \quad (30)$$

The multivariate normal distribution N and the inverted wishart distribution IW [39] have a conjugate property and can be set as the prior PDF $\pi(\theta)$ of the unknown parameters $\theta = [\beta_1, \dots, \beta_M, \sigma_\epsilon, \Sigma_v, \alpha]$. It should be noted that the unknown parameter vector α does not define the prior PDF because the maximum likelihood value can be uniquely obtained by an algebraic calculation when the other parameters are known. This is equivalent to setting an unconditional prior PDF with a uniform probability density [61]. The functional form of the simultaneous posterior PDF $\pi(\theta|\tilde{\mathbf{z}})$ is defined by substituting the likelihood (Eqs. (28) and (30)) and the prior PDF into Eq. (27). This posterior PDF $\pi(\theta|\tilde{\mathbf{z}})$ is then numerically estimated by Gibbs sampling, as described below [45].

2.6. Conditional posterior PDF

MCMC methods numerically obtain the PDF that approximates the simultaneous posterior PDF $\pi(\theta|\tilde{\mathbf{z}})$ [61]. The present study adopts an MCMC approach called the Gibbs sampling method [45]. The method is outlined below (refer to [45] for details). The following section discusses only the sampling of the time-varying coefficient β_m in the TVARX model, which newly introduces the Durbin and Koopman smoother (DK smoother).

Gibbs sampling in the TVARX model is performed by randomly drawing from conditional posterior PDFs $\pi(\mathbf{B}_{-1}|\beta_1, \sigma_\epsilon, \Sigma_v, \alpha, \tilde{\mathbf{z}})$, $\pi(\beta_1|\mathbf{B}_{-1}, \sigma_\epsilon, \Sigma_v, \alpha, \tilde{\mathbf{z}})$, $\pi(\sigma_\epsilon|\mathbf{B}, \Sigma_v, \alpha, \tilde{\mathbf{z}})$, and $\pi(\Sigma_v|\mathbf{B}, \sigma_\epsilon, \alpha, \tilde{\mathbf{z}})$ and calculating α conditional on other parameters. \mathbf{B}_{-1} expresses the parameter set obtained by removing β_1 from \mathbf{B} .

Assuming the conjugate prior PDF, β_1 , σ_ϵ , and Σ_v are drawn from the following conditional a posteriori PDFs:

$$\beta_1 \sim N(\beta_{\beta 1}, \Sigma_{\beta 1}) \quad (31)$$

$$\sigma_\epsilon^2 \sim IW(\sigma_{\epsilon 1}^2, v_{\epsilon 1}, M), \quad (32)$$

$$\Sigma_v \sim IW(\Sigma_{v1}, v_{v1}, M - 1), \quad (33)$$

where N and IW denote multivariate-normal and inverse-Wishart distributions, respectively. Note that $\beta_{\beta 1}$, $\Sigma_{\beta 1}$, $\sigma_{\epsilon 1}^2$, $v_{\epsilon 1}$, Σ_{v1} , and v_{v1} are calculated using Bayes' theorem on the prior PDF and likelihood. The mathematical forms are given in [Appendix III](#). The prior PDFs for β_1 , σ_ϵ^2 , and Σ_v are defined as $\pi(\beta_1) = N(\beta_0, \Sigma_{\beta 0})$, $\pi(\sigma_\epsilon^2) = IW(\sigma_{\epsilon 0}^2, v_{\epsilon 0}, M)$, and $\pi(\Sigma_v) = IW(\Sigma_{v0}, v_{v0}, M - 1)$, as described in [Appendix III](#).

When the conditions of the other parameters are known, the maximum likelihood estimate of α is given by

$$\alpha = (\Lambda^T \Lambda)^{-1} \Lambda^T \mathbf{Z}_\alpha \quad (34)$$

$$\Lambda = [\mathbf{A}_1^T, \dots, \mathbf{A}_{M-1}^T] \quad (35a)$$

$$\mathbf{Z}_\alpha = [\tilde{\mathbf{z}}_2 - \mathbf{Z}_2 \beta_2, \dots, \tilde{\mathbf{z}}_M - \mathbf{Z}_M \beta_M] \quad (35b)$$

2.7. DK smoother

For drawing the time-varying coefficient β_m , Fruhwirth-Schnatter [62] and Carter and Kohn [41] proposed a recursive estimation method based on filtering and smoothing theory, which exploits the conjugacy between the prior PDF and likelihood function. Shortly afterward, Jong and Shephard [42] proposed a simulation smoother that draws the coefficient only during the smoothing process, thereby realizing hierarchical Bayesian estimation by the MCMC method. Hierarchical Bayesian estimation in the TVVAR model was also achieved by a simulation smoother [32]. However, although the simulation smoother can estimate the time-varying coefficient at realistic calculation cost, its computational complexity is high. To resolve this problem, Durbin and Koopman [43] utilized the variance independence in the conditional probability, which improves the computational efficiency of the drawing method. In the present study, this approach (called the DK smoother in honor of its proposers) was introduced into the hierarchical Bayesian estimation of the TVARX model. The independence of the variances in conditional probability is discussed in [Appendix IV](#).

The distributions of the DK solver are $\pi(\mathbf{B}, \mathbf{z})$, $E(\mathbf{B}, \mathbf{z})$, and $E(\mathbf{B}^+, \mathbf{z}^+)$. First, the solver recursively draws random vectors $\mathbf{z}^+ = [z_1^+, \dots, z_M^+]$ and $\mathbf{B}^+ = [\beta_1^+, \dots, \beta_M^+]$ from the distribution $\pi(\mathbf{B}, \mathbf{z})$ as follows:

$$z_m^+ \sim N(\mathbf{A}_m \alpha + \mathbf{Z}_m \beta_m, \sigma_\epsilon^2) \quad (36)$$

$$\beta_{m+1}^+ \sim N(\beta_m^+, \Sigma_v) \quad (37)$$

Next, $\widehat{\mathbf{B}} = E(\mathbf{B}|\mathbf{z})$ is calculated by recursive computation of Eq. (40) after filter and smoother processing (given by Eqs. (38) and (39), respectively).

$$\begin{aligned} v_m &= z_m - \mathbf{Z}_m \beta_m, \\ F_m &= \mathbf{Z}_m \Sigma_{\beta, m} \mathbf{Z}_m^T + \sigma_\epsilon^2, \\ \mathbf{K}_m &= \Sigma_{\beta, m} \mathbf{Z}_m^T F_m^{-1}, \\ \mathbf{L}_m &= \mathbf{E} - \mathbf{K}_m \mathbf{Z}_m, \\ \beta_{m+1} &= \beta_m + \mathbf{K}_m v_m, \\ \Sigma_{\beta, m+1} &= \Sigma_{\beta, m} \mathbf{L}_m^T + \text{chol}(\Sigma_v), \end{aligned} \quad (38)$$

$$\mathbf{r}_{m-1} = \mathbf{Z}_m F_m v_m + \mathbf{L}_m^T \mathbf{r}_m. \quad (39)$$

$$\hat{\beta}_{m+1} = \hat{\beta}_m + \text{chol}(\Sigma_v) \mathbf{r}_m \quad (40)$$

where $\text{chol}(\cdot)$ denotes Cholesky decomposition and \mathbf{E} denotes the unit matrix.

$\hat{\mathbf{B}}^+ = E(\mathbf{B}^+ | \mathbf{z}^+)$ is obtained by the same calculation, but replacing \mathbf{B} and \mathbf{z} in Eqs. (38)–(40) with \mathbf{B}^+ and \mathbf{z}^+ , respectively. Finally, after inserting $\hat{\mathbf{B}}$, \mathbf{B}^+ , and $\hat{\mathbf{B}}^+$ into Eq. (41), the samples can be efficiently drawn from the conditional probability $\pi(\mathbf{B} | \sigma_\epsilon, \Sigma_v, \alpha, \tilde{\mathbf{z}})$.

$$\mathbf{B} = \hat{\mathbf{B}} + \mathbf{B}^+ - \hat{\mathbf{B}}^+ \quad (41)$$

Note that in the actual applications of the DK smoother, the time-varying coefficients β_m and observed values \mathbf{z}_m are initialized to β_0 and $\tilde{\mathbf{z}}_m - \mathbf{Z}_m \beta_0$ ($m = 1, \dots, M$), respectively.

2.8. Estimation procedure

This subsection summarizes the Gibbs sampling estimation with the above-formulated DK smoother. The right superscript of each variable denotes the number of sampling times of that variable.

Step 1 From the displacement response during train passage, specify the speed v and entry time of the train on the bridge. Set the exogenous variables by calculating \mathbf{A}_m ($m = 1, \dots, M$) using Eq. (4). Initialize the unknown parameters $\mathbf{B}^{(0)}$, $\sigma_\epsilon^{(0)}$, and $\Sigma_v^{(0)}$. These initial values can be set to their normal, time-invariant ARX estimation results. Set the parameters β_0 , $\Sigma_{\beta 0}$, $\sigma_{\epsilon 0}^2$, v_{e0} , Σ_{v0} , and v_{v0} of the prior PDF; the number of iterations until convergence to steady-state \bar{n} (the burn-in period); and the maximum number of iterations n and iteration number n_g are set to 1.

Step 2 Draw $\beta_1^{(n_g)}$ at iteration number n_g from Eq. (31).

Step 3 Draw $\mathbf{B}^{(n_g)}$ at iteration number n_g by the DK smoother expressed by Eqs. (38)–(40).

Step 4 Using $\mathbf{B}^{(n_g)}$ and $\tilde{\mathbf{z}}$, calculate $\alpha^{(n_g)}$ at iteration number n_g using Eq. (34).

Step 5 Draw $\sigma_\epsilon^{(n_g)}$ at iteration number n_g from Eq. (32).

Step 6 Draw $\Sigma_v^{(n_g)}$ at iteration number n_g from Eq. (33).

Step 7 If $n_g > \bar{n}$ for sufficiently large \bar{n} , record $\theta^{(n)} = [\mathbf{B}^{(n)}, \sigma_\epsilon^{(n)}, \Sigma_v^{(n)}, \alpha^{(n)}]$.

Step 8 If $n_g = n$, go to Step 9. If $n_g < n$, update $n_g = n_g + 1$, and return to Step 2.

Step 9 Calculate the expected value of $\beta_m^{(\bar{n}+1, \dots, n)}$ at each time point m , and estimate the value of $\hat{\beta}_m$. Using the obtained $\hat{\beta}_m$, estimate the instantaneous natural frequency \hat{f}_m and the instantaneous modal damping ratio $\hat{\xi}_m$ using Eqs. (22)–(24).

The proposed algorithm was implemented in Matlab ver. 9.3.0 (R2017b) [63]. In most of the displacement responses (both simulated and real), the posterior PDF converged within 500 iterations (as described later). In the workstation environment (Core i7 to 6850 K, 3.60 GHz, mounting memory 32 GB, 64 bit OS), 5000 iterations of the test data were usually completed in 40–45 s. The test data contains time-history response of 5000 samples with 0.02-s increments. In the same environment, the TVVAR model of Ref. [32] required 700–750 s to calculation with the same data. Clearly, the DK smoother greatly accelerates the hierarchical Bayesian estimation and reduces the computational cost.

3. Verification by numerical calculation

3.1. Setup for TVARX model estimation

This subsection conducts the verification step (the first V of the so-called V & V (Verification and Validation) process [64]) in numerical calculations. First, the instantaneous natural frequency f_m and the instantaneous modal damping ratio ξ_m are set assuming arbitrary variations, and the time-varying coefficient β_m is back-calculated from these instantaneous parameters. These three values are set as the exact values. The bridge displacement response \tilde{z} is simulated by TVARX model given the calculated time-varying coefficient β_m and the modal external force $\sum A_{i,t}$. The passing train comprises eight vehicles, and the TVARX model is free of observation error. The obtained bridge displacement response \tilde{z} and the modal external force $\sum A_{i,t}$ provide as the input response and exogenous variables for the proposed estimation method. From the estimated time-varying coefficient $\hat{\beta}_m$, the instantaneous natural frequency \hat{f}_m and the modal damping ratio $\hat{\xi}_m$ are recalculated using

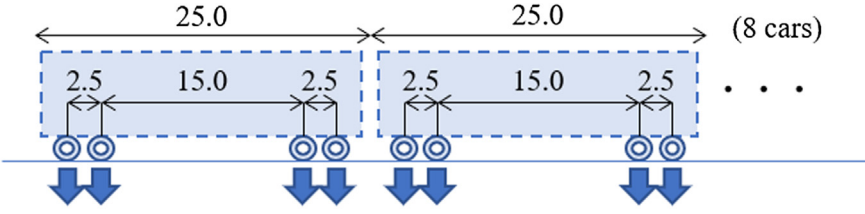


Fig. 5. Vehicle axis arrangement (m).

the hierarchical Bayesian estimation. The estimation accuracy of the proposed method is verified by comparing the simulated and exact results.

The railway bridge had a span length of 25 m, a natural frequency of 2.7 Hz, a damping ratio of 0.02, and a unit-length mass of 22 t/m. The train passing speed (230 km/h) was close to the resonance speed, and each of the eight vehicles was 25 m long. The wheelset arrangement is shown in Fig. 5. The instantaneous natural frequency f_m and modal damping ratio ξ_m were set as shown in Eq. (42). With each wheelset passage, f_m reduced by 5%, whereas ξ_m increased by 20%.

$$f_m = 2.7 - 0.135 \sum_{i=1}^{32} A_{i,m} \xi_m = 0.02 + 0.004 \sum_{i=1}^{32} A_{i,m} \quad (42)$$

Fig. 6 shows the created input response $\tilde{\mathbf{z}}$, exogenous variables $\sum A_{i,t}$, instantaneous natural frequency f_m , instantaneous modal damping ratio ξ_m , and time-varying coefficient β_m . The instantaneous natural frequency and the instantaneous power spectrum calculated from the time-varying coefficient β_m are shown in Fig. 7. Panels (a) and (b) of Fig. 6 are input to the hierarchical Bayesian estimation. The burn-in was set to 2000 iterations, and the maximum iteration number was 5000. The parameters were initialized to their estimated values in the ARX model. The prior PDF parameters are set as 1.946 and -0.9932 for $\beta_0 = [\beta_1, \beta_2]$ based on the ARX model estimation results. Other prior PDF parameters are set as 0.001^2 and 0 for the diagonal and nondiagonal components of $\Sigma_{\beta 0}$, respectively, 0.001 for σ_{e0}^2 , 1 for ν_{e0} , 0.001 and 0 for diagonal and non-diagonal components of Σ_{v0} , and 0.01 for ν_{v0} . These values were adopted to avoid the overconstraint of the large variances relative to the averaged values and actual time-varying variation. This prior PDF parameter setting is commonly used for the application of the VBI simulation and measured responses.

3.2. Estimation results and comparison with the existing methods

Fig. 8 shows the hierarchical Bayesian estimation results of the TVARX model. The time-varying coefficients $\hat{\beta} = [\hat{\beta}_1, \hat{\beta}_2]$ were accurately estimated, and the input displacement response of the hierarchical Bayesian TVARX model matched the

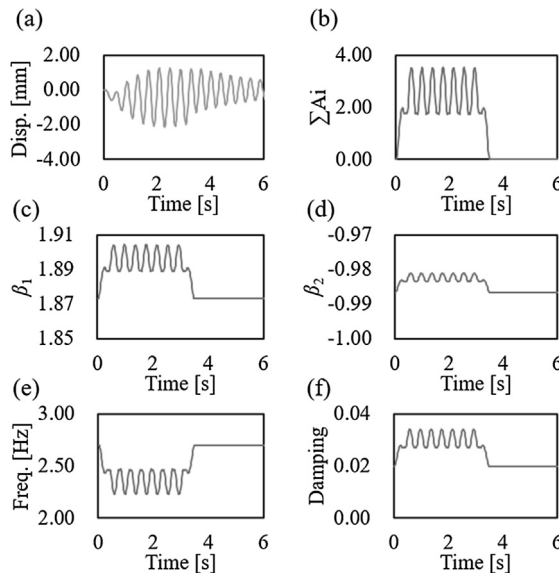


Fig. 6. Input responses and exact results for verifying the proposed method: (a) input displacement response, (b) exogenous variables, (c) exact time-varying coefficient β_1 , (d) exact time-varying coefficient β_2 , (e) exact natural frequency, and (f) exact modal damping ratio.

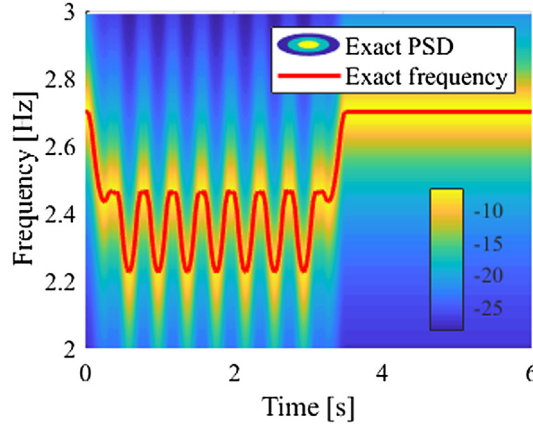


Fig. 7. Exact values of instantaneous power spectrum and natural frequency.

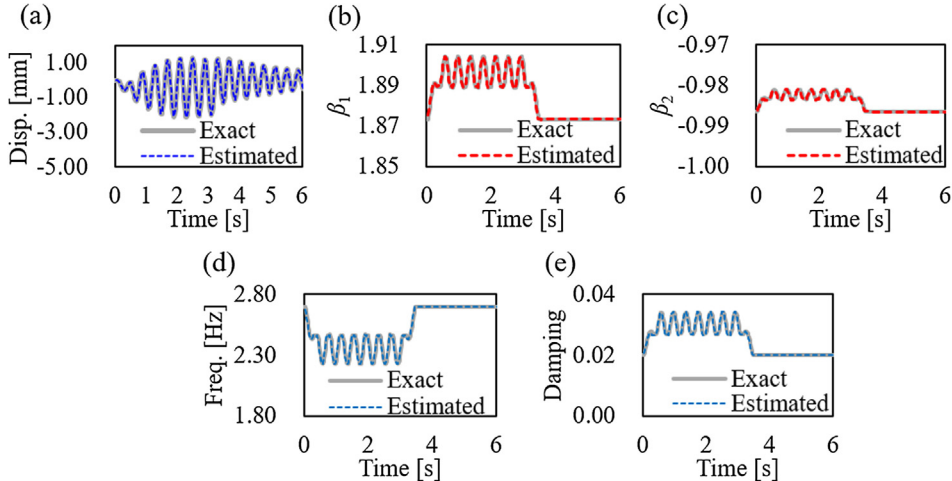


Fig. 8. Estimated results of the proposed TVARX model; (a) displacement response, (b) time-varying coefficient β_1 , (c) time-varying coefficient β_2 , (d) natural frequency, and (e) modal damping ratio.

exact response (Fig. 8(a)–(e)). Consequently, the instantaneous natural frequency \hat{f}_m and modal damping ratio $\hat{\xi}_m$ were also estimated with high accuracy. In addition, the estimated instantaneous power spectrum in Fig. 9 coincided with the exact spectrum shown in Fig. 7. Therefore, the proposed methodology can evaluate the variations in the natural frequency and modal damping ratio of a resonant bridge under the external force exerted by a passing train.

To verify the effectiveness of the proposed method, the same displacement response was computed by the hierarchical Bayesian estimation in the TVVAR model, proposed for time–frequency analysis in an earlier study. The TVVAR model (detailed in [32]) is a time-varying time-series model with white noise (the external force). The results are shown in Figs. 10 and 11. The natural frequency and modal damping ratio were estimated more accurately in TVVAR than by time–frequency analysis based on short-time Fourier transformation [32]. Although the TVVAR model accurately estimated the displacement response (Fig. 10(a)), the instantaneous natural frequency \hat{f}_m , instantaneous modal damping ratio $\hat{\xi}_m$, and the time-varying coefficients $\hat{\beta}_m$ largely deviated from their exact values (Fig. 10(b)–(e)). This confirms that the periodicity of the external force largely affects the estimated displacement response of a resonant bridge. As shown in the estimated instantaneous power spectrum (Fig. 11), the natural frequency estimated by the TVVAR model also greatly varies. In the resonance situation, the dominant frequency of the external force approaches the natural frequency of the railway bridge. As the TVVAR model cannot separate the two effects, it generates large estimation errors. Conversely, the proposed TVARX model avoids the error caused by the external force and separates the bridge time–frequency characteristics from the input characteristics.

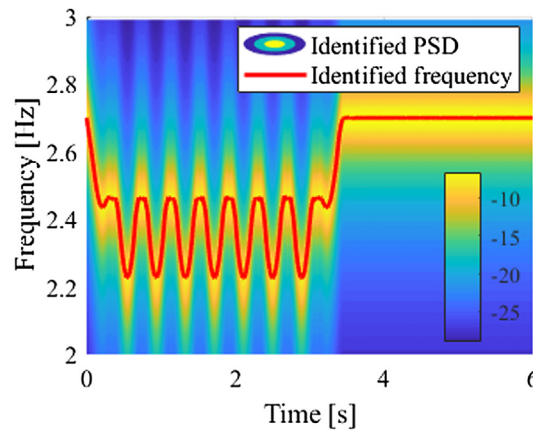


Fig. 9. Instantaneous power spectrum estimated by the proposed method.

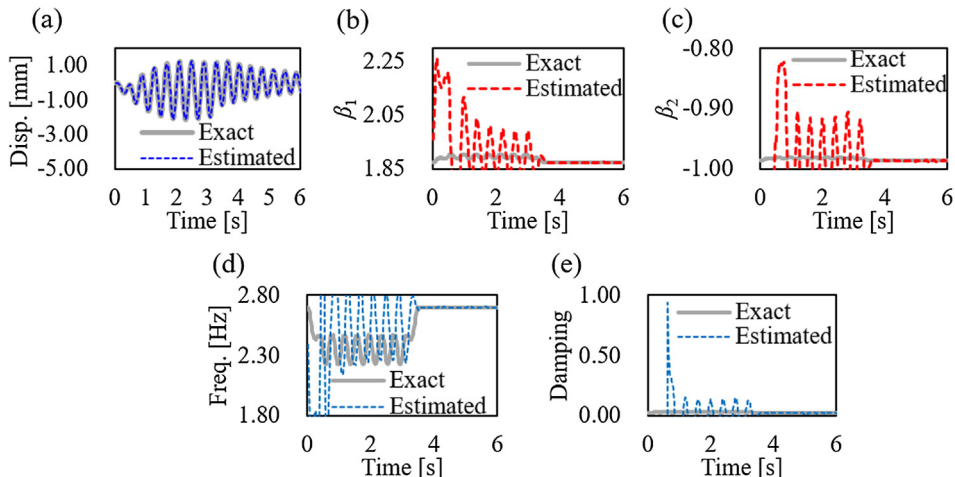


Fig. 10. Estimated results of previous method (TVVAR model); (a) displacement response, (b) time-varying coefficient β_1 , (c) time-varying coefficient β_2 , (d) natural frequency, and (e) modal damping ratio.

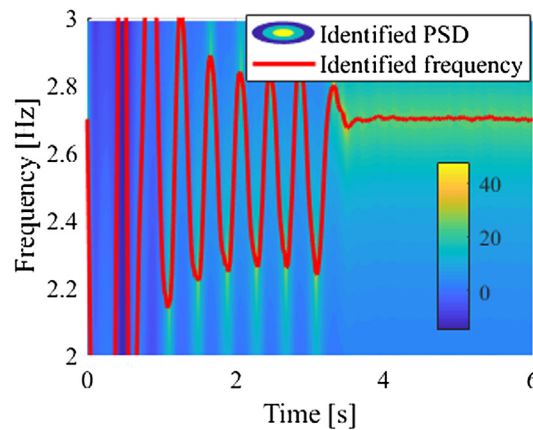


Fig. 11. Estimated result of instantaneous power spectrum (TVVAR model).

3.3. Influence of the observation noise impact

Next, normally distributed noise was added to the displacement response shown in Fig. 6(a) and input to the TVARX model. Random numbers were generated from the normal distribution and displaced by 1%, 2%, and 5% from the average (representing standard deviations). During train passage, these noises were added to the displacement response. In the image capture displacement measurements, the error was approximately 2% of the average displacement. The measurement accuracy of this method is comparatively low. The burn-in and maximum number of iterations in the MCMC were set to 2000 and 5000, respectively. The initial values were the estimated values of the ARX model. In addition, the setting of a prior PDF is the same as mentioned in Section 3.1. The results were evaluated by their average error AE . For example, the average error of the natural frequency AE_f was calculated as follows:

$$AE_f = \frac{1}{n_{Train}} \sum_{m=1}^{n_{Train}} \left| \frac{f_m - \hat{f}_m}{f_m} \right| \quad (43)$$

where n_{Train} is the number of samples during a train passage. The average errors of the other estimated results (modal damping ratio, time-varying coefficients, and the displacement responses) were calculated using similar formulas.

Table 1 summarizes the average errors in the estimation results of the proposed method with noisy inputs. For comparison, the results of the TVVAR model (see Fig. 10) are also presented. At noise levels below 2%, the TVARX model estimated the time-varying coefficients $\hat{\beta}_m$ to within 0.5% of their correct values. However, when the additional noise increased to 2%, the average error of the instantaneous modal damping ratio reached nearly 30%. Therefore, for accurate estimates of instantaneous modal damping, the error in the displacement measurement method must be small. In contrast, the TVARX estimation of instantaneous natural frequency was relatively robust to observation noise, with an average error of approximately 5% under an additional noise of 5%. The hierarchical Bayesian estimation of the noisy TVARX model more accurately estimated the instantaneous natural frequency and modal damping ratio than TVVAR without noise, even when the added noise was increased to 5%.

3.4. Time synchronization error impact

When applying the model to real bridge responses, the speed and timing of the train entering the bridge must be accurately specified because the modal external force is the inputted exogenous variable (Fig. 6(b)). However, in reality, few measurement systems can accurately identify the time at which a train enters a bridge. Therefore, time synchronization error in the exogenous variable is almost inevitable. To evaluate how this asynchronous error affects the estimation results, the TVARX method was evaluated on shifted time points of the modal external force. The synchronization error was varied as ± 0.01 , ± 0.02 , and ± 0.04 s, corresponding to 0.5, 1, and 2 samples of the observed data (at a 50 Hz sampling rate), respectively.

Table 2 summarizes the average errors in the estimation results of the proposed method with synchronization error in the input. The time synchronization error mainly affected the instantaneous modal damping ratio, especially when the exogenous variable was input earlier than the actual time. Furthermore, the error rapidly increased when the time synchronization error exceeded ± 0.02 . Therefore, to accurately estimate the instantaneous modal damping ratio, the time synchronization must be within ± 0.01 s of the true time synchronization. If the measurement is sampled at 50 Hz, the time synchronization error corrected by simple cross-correlation is within ± 0.01 s at least. Therefore, the proposed method is expected to require no complex time synchronization processing, such as interpolation and resampling, in real applications.

4. Validation by VBI simulation

4.1. Setup for VBI model

In Section 3, basic influential factors, such as noise and time synchronization, were verified. However, the dynamic response of the railway bridges under the passage of a train is influenced by various parameters apart from the moving load's effect on the traveling vehicle considered by TVARX. The train speed is the resonance speed because this study deals with the resonance situation when the VBI effect becomes the largest. However, setting the exact train speed during actual measurement is difficult; thus, it is necessary to clarify the influence of the train speed on the estimation result. In addition,

Table 1

Average errors of the estimation results by proposed method based on the input with added noise (span length 25 m, train speed equivalent to 230 km/h) [%].

Added noise	Displacement response	Instantaneous natural frequency	Instantaneous modal damping ratio	β_1	β_2
0%	0.0	2.4	0.1	0.2	0.1
1%	2.5	3.4	10.3	0.3	0.4
2%	4.6	3.8	27.1	0.3	0.4
5%	12.1	5.5	68.9	1.1	1.4
TVVAR w.o. noise	0.5	17.7	793.0	5.3	9.3

Table 2

Summarizes average errors of the estimation results by proposed method based on the input with synchronization error (span length 25 m, train speed equivalent to 230 km/h) [%].

Synchronization error	Displacement response	Instantaneous natural frequency	Instantaneous modal damping ratio	β_1	β_2
0 s	0.0	2.4	0.1	0.2	0.1
+0.01 s	0.1	2.4	3.1	0.3	0.3
+0.02 s	0.1	2.4	38.1	0.5	0.7
+0.04 s	0.6	4.4	61.7	0.8	1.1
-0.01 s	0.1	2.4	8.5	0.5	0.5
-0.02 s	0.1	2.5	76.6	0.7	1.3
-0.04 s	0.2	3.3	144.6	1.3	2.5

rail irregularity is an influential factor that cannot be avoided in real bridges. Here, the bridge displacement responses during the passage of a train are calculated using the VBI model. The influences of the train speed and rail irregularity on the estimation results are clarified, and the applicability of the proposed method is also verified.

The target bridge has the same specifications as those in the verification in Section 3. The railway bridge had a span length of 25 m, a natural frequency of 2.7 Hz, a damping ratio of 0.02, and a unit-length mass of 22 t/m. The train is assumed to be 8 vehicles with a 25-m length, which is a typical high-speed railway in Japan. The wheelset arrangement is shown in Fig. 5. The physical specifications of the vehicle were set as follows with reference to the past literature [2,3,65]. The car body mass is 34 t, car body pitching rotational inertia is 2000 tm^2 , bogie mass is 3 t, bogie pitching rotational inertia is 4 tm^2 , wheelset mass is 2 t, secondary spring is 500 kN/m, secondary damper is 100 kNs/m, primary spring is 1000 kN/m, and primary damper is 40 kNs/m. The response was calculated in steps of 0.001 s in the VBI simulations. The resulting displacement responses at the mid-span of the bridge were resampled in steps of 0.02 s and used as the input for the TVarX model.

4.2. Train speed

To investigate the influence of the train speed, the train speed v was set to 80%, 90%, 95%, 105%, 110%, 120% ($0.8v_{\text{res}}, 0.9v_{\text{res}}, 0.95v_{\text{res}}, 1.05v_{\text{res}}, 1.1v_{\text{res}}, 1.2v_{\text{res}}$) of the resonance speed $v = v_{\text{res}} = 240 \text{ km/h}$. The resonance train speed was set as the speed at which the resonance curve showed a peak using VBI simulation and the train speed as the parameter. Fig. 12 denotes the resonance curve calculated by the VBI model, the ML model, and the target train speed for the proposed method. When compared with the ML model, the resonance curve of the VBI model has a smaller maximum value near the resonance speed. Also, the resonance speed of the VBI model is slightly lower than that of the ML model. Therefore, the displacement responses obtained by the VBI model include additional damping effects and additional mass effects.

Fig. 13 shows the displacement responses and the modal external force $\sum A_{i,t}$ of the target train speed cases. In case of a resonance speed of 5%, displacement gradually increases when a train passes. At resonance speeds of $\pm 10\%$ and $\pm 20\%$, a beat phenomenon occurred in which the amplitude increased and decreased during the passage of a train.

The parameters of the TVarX model were estimated by hierarchical Bayesian method with these displacement responses and modal external force $\sum A_{i,t}$ as input. For all the responses, burn-in was performed 2000 times, and sampling end was performed 5000 times. The initial value was the estimated value of the ARX model. In addition, the setting of a prior PDF is the same as mentioned in Section 3.1.

Fig. 14 denotes the estimation results of the displacement responses, instantaneous natural frequencies, and instantaneous modal damping ratios at various train speeds. The displacement responses are also shown with the calculation result of the VBI model used as the input. The proposed method estimates the displacement responses to fit the input of any speed. For instantaneous natural frequencies, it is possible to confirm the long-periodic decreasing behavior corresponding to the entire train transit period and the instantaneous fluctuation behavior corresponding to the passage of each vehicle. The long-periodic decrease of the natural frequency shows an approximate decrease of 1% from 2.7 Hz to approximately 2.67 Hz.

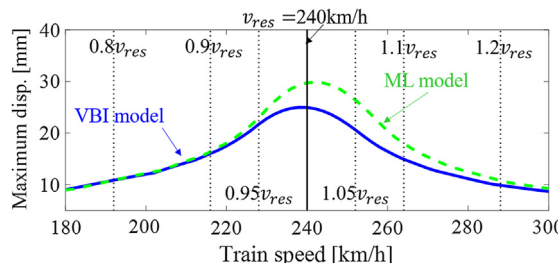


Fig. 12. The maximum displacement of the train speed function calculated by the VBI model and the train speed used for verifications.

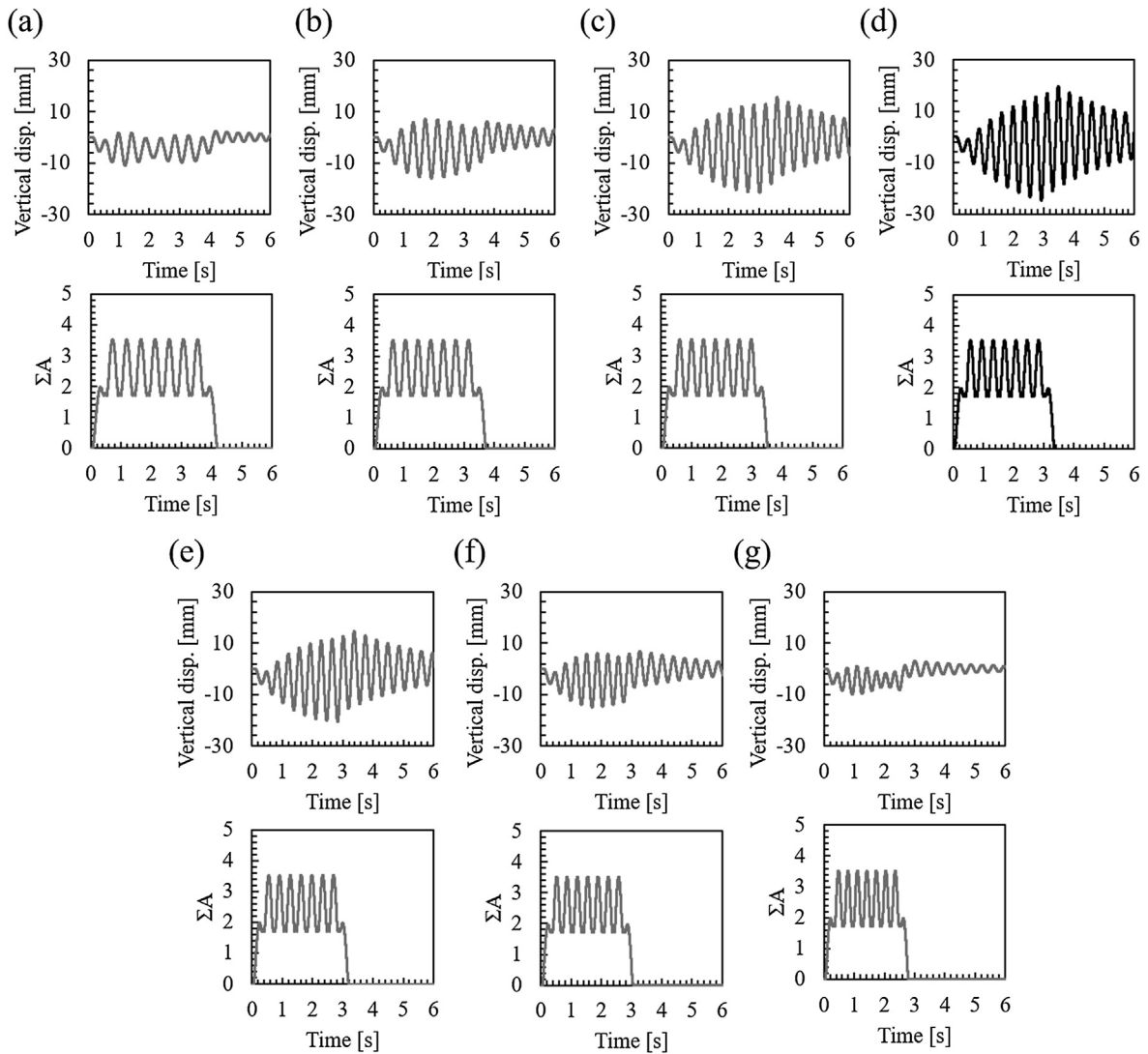


Fig. 13. Bridge displacement and modal external force calculated by VBI model at train speeds of (a) 192 km/h, (b) 216 km/h, (c) 228 km/h, (d) 240 km/h, (e) 252 km/h, (f) 264 km/h, and (g) 288 km/h.

However, the increase and decrease in natural frequencies with the passage of each vehicle are the largest around the resonance speed (228–264 km/h). In addition, the natural frequencies fluctuate more considerably when the final vehicle passes when compared with that observed when the first vehicle passes. The fluctuation amplitudes associated with these passing vehicles decrease as the train speeds are quite different from the resonance speed. In Fig. 14 (a), (b) and (f), (g), the amplitude during train passing increases or decreases owing to beating. Further, the timing at which the amplitude of the instantaneous natural frequency fluctuation increases and the timing at which the amplitude increases due to the beat coincide. Similarly, in case of the instantaneous modal damping ratio, it is possible to confirm the long-periodic increase corresponding to the entire train transit period and the instantaneous increase component accompanying the passage of each vehicle. Furthermore, it is possible to confirm the tendency that the fluctuation accompanying the vehicle passage increases when the amplitude increases due to the beat such as the natural frequency. When the displacement response increases due to the beat and resonance, the phases of the passing axle of the traveling train and the natural vibration of the bridge coincide. Therefore, it is inferred that the VBI effect due to the coupling with the vehicle system changes with the phase of the natural vibration of the bridge when each axle of the vehicle passes the bridge. This is in addition to the members and vibration characteristics of the traveling vehicle. Such a phenomenon is uniquely obtained by the proposed method that can analyze the time-varying modal characteristics of resonance, and this is an example showing the effectiveness of the analysis of the VBI effect using the proposed method. Fig. 14(a) and (g) show the train speeds having a resonance speed $\pm 20\%$, revealing small drifts after the passing trains cause no fluctuation. The estimation accuracy of the instantaneous natural frequency and the instantaneous

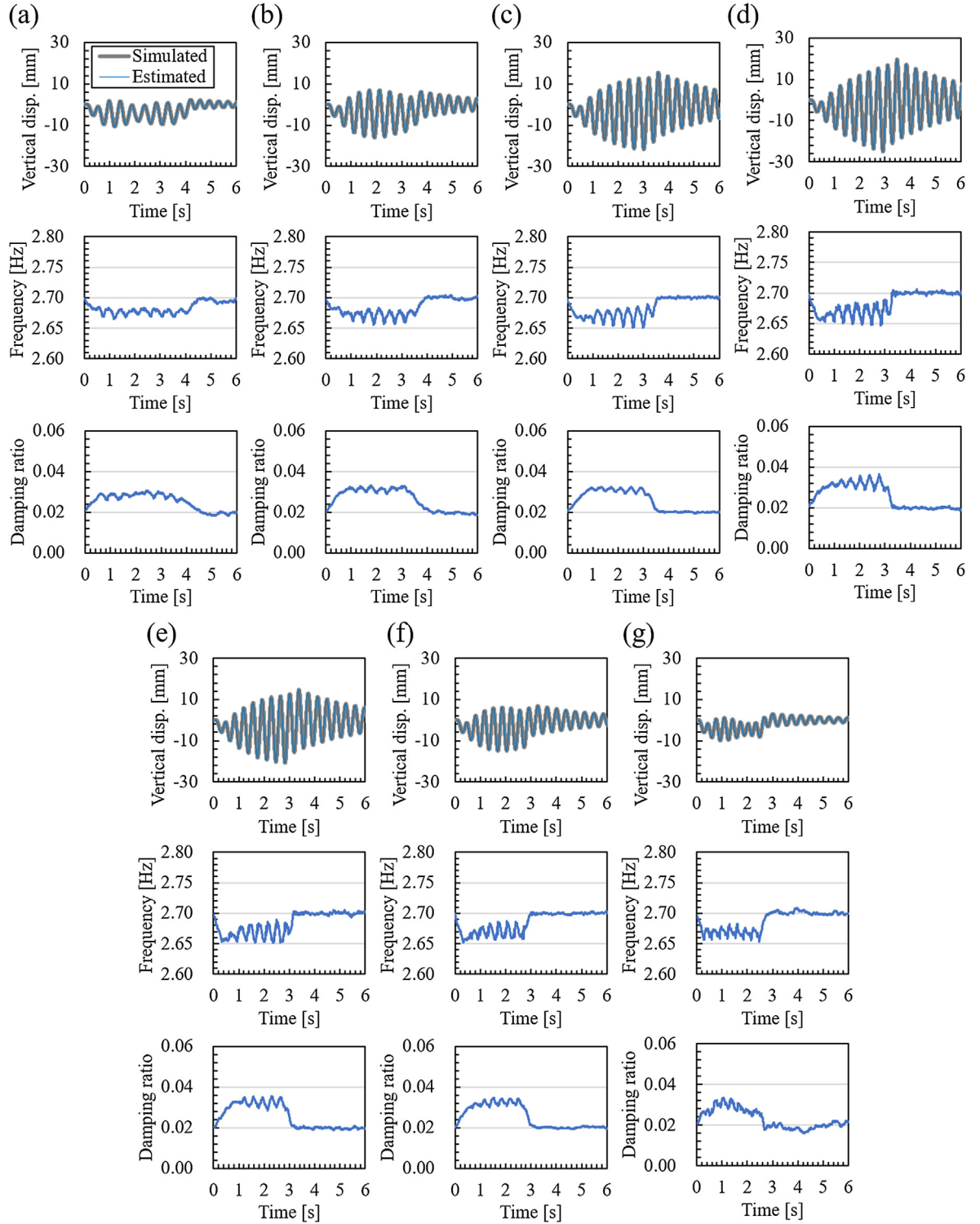


Fig. 14. Estimated results of bridge displacements, instantaneous natural frequencies, and modal damping ratios at train speeds of (a) 192 km/h, (b) 216 km/h, (c) 228 km/h, (d) 240 km/h, (e) 252 km/h, (f) 264 km/h, and (g) 288 km/h.

modal damping ratio during the passage of a train may be degraded at these train speeds. Because these speeds are far from the resonance speed, the dynamic response components of the bridge to estimate the AR coefficients are small when compared with those in other cases. Thus, it is desirable to target train speeds up to approximately $\pm 10\%$ of the resonance speed

for analyzing the VBI effect of the proposed method. The range of $\pm 10\%$ resonance speed, which is the application range, overlaps with the region, where the error of the linear system identification method becomes large due to the VBI effect. Despite the limitations of the scope of application, the proposed method is still effective in the evaluation of VBI effects and the accuracy of SHM.

4.3. Rail irregularity

VBI simulations are performed by considering the rail irregularities created by numerical calculation. The proposed method is applied to the displacement responses. This is calculated by the VBI simulation considering the rail irregularities, and the effect is verified by comparing it with the estimation result based on the displacement response without rail irregularity. The train speed is 240 km/h, which is the resonance speed.

The rail irregularities were characterized by Wiriachai et al. [66] as one-sided power spectral density function (PFD) $S_{rr}(\Omega)$, where $\Omega = 2\pi/L_r$ rad/m is the spatial frequency or wave number. L_r is the wavelength of the rail irregularity. This study employed Eq. (45) proposed by Zhang et al. [67] and Lei and Noda [68] based on Wiriachai et al. [66].

$$S_{rr}(\Omega) = kA \frac{\Omega_c^2}{(\Omega^2 + \Omega_c^2)\Omega} \quad (45)$$

where $k = 0.25$, $\Omega_c = 0.8245$ rad/m. The value of coefficient A is presented in Table 3.

The previously measured results on Japanese high-speed railway have shown that the maximum amplitude of rail irregularities is within ± 7 mm. In recent years, the measured value of a 40-m chord value (relative displacement with respect to the average value at 20-m points front and back of a target point) is a maximum of approximately 5 mm [69,70]. These values correspond to Grade 6 when compared with the values in Eq. (45) and Table 3 [70]. For high-speed railways, Grade 6 and Grade 5, which were more severe, were considered as rail irregularities. To consider the randomness of rail irregularities, 10 rail irregularities were generated for each of Grade 5 and 6, and the influence on the estimation accuracy of the proposed method was examined.

Fig. 15 denotes the rail irregularities of Grade 5 and Grade 6 considered for VBI simulation. The bridge is located at 0–25 m in the figure. The total amplitude is approximately 10–15 mm and 5–7 mm for Grade 5 and Grade 6, respectively. To sufficiently excite the vehicle vibration, rail irregularities were generated up to 200 m before the bridge, and the vehicle passed the bridge after traveling these pre-running sections. Fig. 16 shows the vertical displacement responses at the mid-span of the bridge. The calculation considers the rail irregularities. The difference in the maximum displacement was approximately $\pm 3\%/\pm 1\%$ for Grade 5/Grade 6 rail irregularity, respectively.

The parameters of the TVARX model were estimated by the hierarchical Bayesian method with the displacement responses and modal external force $\sum A_{i,t}$ as inputs. For all the responses, burn-in was performed 2000 times and sampling end was conducted 5000 times. The initial value was the estimated value of the ARX model. In addition, the setting of a prior PDF is the same as 3.1.

Figs. 17 and 18 denote the effect of rail irregularity on the instantaneous natural frequency and the instantaneous modal damping ratio estimated by the proposed method. The instantaneous natural frequency, shown in Fig. 17, indicates that the difference due to the presence or absence of rail irregularities appears mainly at 1.5–2.5 s corresponding to the passing of the first and second vehicles. In particular, when passing through the connection part of the first and second vehicles at 1.7–1.8 s, the difference due to rail irregularity is maximized. This difference is larger in Grade 5 when compared with that in Grade 6. However, the effect of rail irregularity is smaller after the passage of the third vehicle. During resonance, the dynamic response of the bridge is gradually amplified as the vehicle passes. Therefore, the estimation error due to the rail irregularity has a relatively large effect when the first and second vehicles pass in which the dynamic response of the bridge is insufficiently excited. Even in case of a railway bridge resonance, it is necessary to pay attention to the rail irregularity errors in case of the first and second vehicles whose dynamic response is insufficiently excited. However, Fig. 18 shows that the effect of rail irregularities on the estimation results of the instantaneous modal damping ratio is small. It is inferred that the difference in the effect on rail irregularities between the instantaneous natural frequency and the instantaneous modal damp-

Table 3
Coefficients A of the rail irregularity power spectrum density.

Grade	Coefficients A
1	121.07
2	101.81
3	68.16
4	53.76
5	20.95
6	3.39

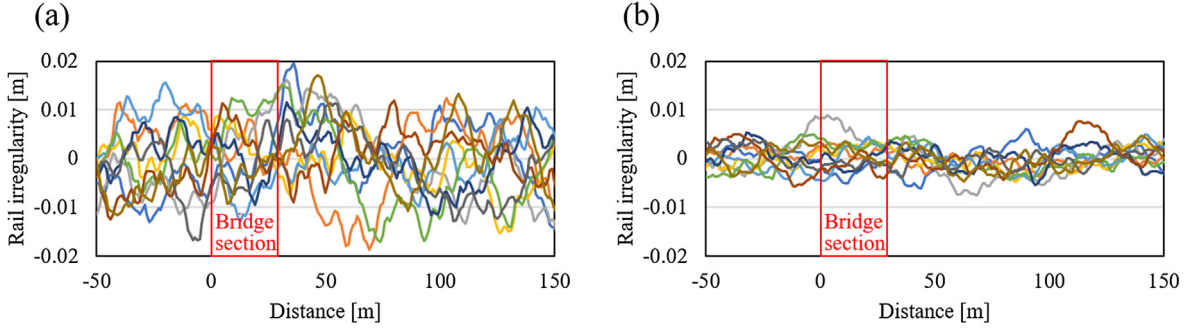


Fig. 15. Rail irregularities introduced in VBI simulations: (a) Grade 5 and (b) Grade 6.

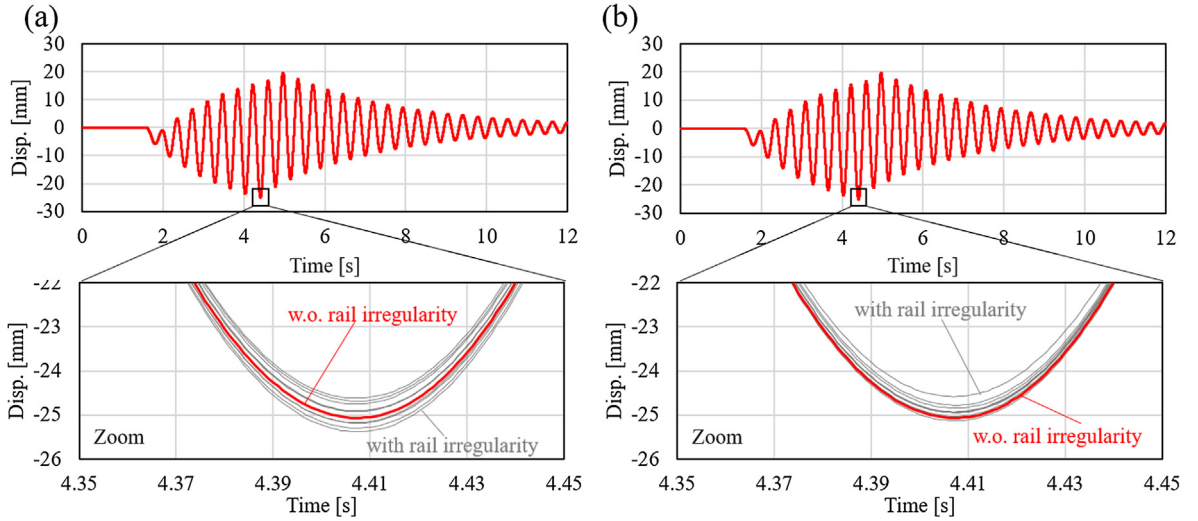


Fig. 16. VBI simulation results of displacements in consideration with the rail irregularity of (a) Grade 5 and (b) Grade 6.

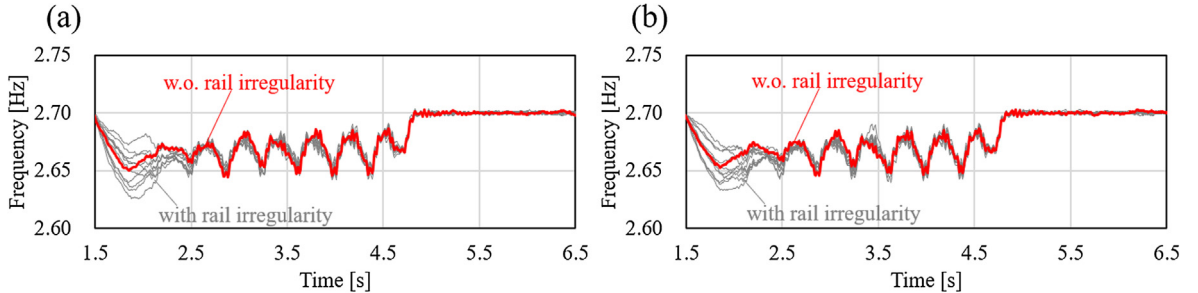


Fig. 17. Estimation results of instantaneous natural frequency considering the rail irregularity: (a) Grade 5 and (b) Grade 6.

ing ratio depends on the members of the vehicle supplying the VBI effect and the sensitivity of those members to the rail irregularities. A detailed study on vehicle components contributing to the VBI effect is beyond the scope of this study. However, the trend can be analyzed using the proposed method and VBI simulation.

5. Application to the actual bridges

In this section, the proposed method is tested against the measured displacement responses of resonant bridges under prominent VBI effects. These measurements provide the actual instantaneous natural frequency and instantaneous modal damping ratio. The proposed method is further tested in simulated displacement responses of VBI models, with the vehicle

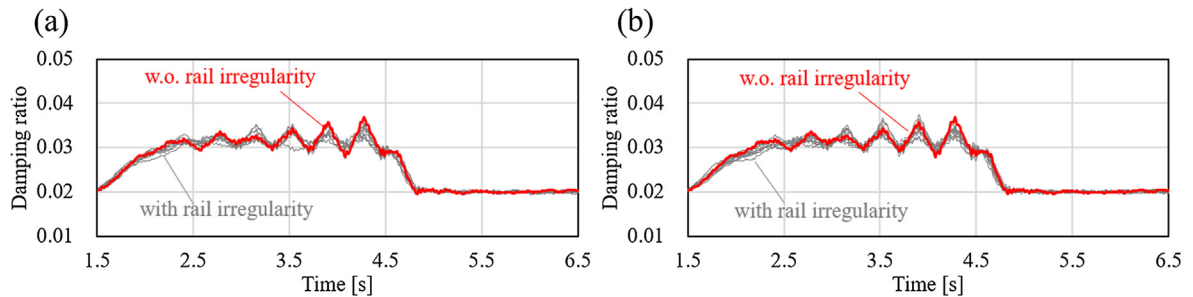


Fig. 18. Estimation results of instantaneous modal damping ratio considering the rail irregularity: (a) Grade 5 and (b) Grade 6.

and bridge parameters adjusted to match the measurement results. The accuracy of the additional mass and damping effects in the VBI model is also verified. The applied displacement responses were measured in the speed improvement tests before opening the high-speed railway. The rail irregularities were managed in all the tests [69,70].

5.1. Target bridges and measurement setup

By applying the hierarchical Bayesian estimation of the TVARX model to the measured response, we can verify the applicability of the proposed method under actual measurement conditions, such as noise and time synchronization, and also reveal the VBI effect in actual resonant bridges.

Table 4 shows the specifications of the target bridges analyzed in this study. From the accumulated resonance responses during actual train passage, we selected five bridges in which the first to third resonances occurred at train speeds of up to 260 km/h. The span lengths ranged from approximately 9 to 60 m. The measured natural frequencies and modal damping ratios were identified from the measured responses after train passages as described in [71].

Fig. 19 shows the cross-section of bridge #1 and its measurement setup. As shown in **Fig. 19(b)**, the displacement responses were measured using a ring-type displacement meter installed at the mid-span and by contact-type displacement meters installed at both bearing parts. When the girder deflected, the displacement responses at the mid-span were accurately measured by removing the bearing subsidence. Moreover, the displacement component caused by torsional deformation was removed by averaging the displacements during the up- and down-bound train passage. However, the resonant response was dominated by the first bending mode, and the torsional component was negligible under this condition [1].

5.2. Preprocessing

Prior to applying the TVARX model, the timing was synchronized by cross-correlation, and the modal external forces $\sum A_{i,t}$ were set for each response. The axle arrangement of the vehicles (regardless of type) is shown in **Fig. 5**. The speed and entry timing of the train on the bridge, which significantly influence the TVARX estimation results, were estimated by grid searching over measured values of ± 3 km/h (in 0.1 km/h increments) and ± 0.3 s (in 0.01 s increments), respectively. The setting of the prior PDF is the same as 3.1. The burn-in was set to 2000 iterations, and the maximum number of iterations was 5000.

The proposed method was also evaluated on displacement response simulated by the VBI model without rail irregularity and spatial stiffness parameter changes. The parameters of the VBI model were adjusted so that the simulated displacement responses matched the measured ones. By comparing the instantaneous natural frequencies or modal damping ratios in the measured and numerical displacement responses, one can verify the assumption such as the bridge without rail irregularity and spatial stiffness parameter changes. The initial values and number of iterations in the hierarchical Bayesian estimation were set to match the initial responses with the measured ones.

Table 4
Properties of the analyzed bridges.

ID	Purpose	Girder type	Span [m]	Unit length mass [kg/m]	Measured frequency[Hz]	Measured damping	Car #	Resonance Speed* [kg/h]	Measured Speed [kg/h]
#1	1st resonance	Through	58.2	50,000	2.97	0.024	10 cars	262	255
#2	1st resonance	Box	50.7	42,000	2.98	0.022	10 cars	268	256
#3	1st resonance	T	45.6	36,000	2.72	0.032	10 cars	245	260
#4	2nd resonance	Hollow	24.2	32,000	4.54	0.018	10 cars	409	208**
#5	3rd resonance	T	9.3	10,000	8.30	0.024	12 cars	770	257***

*: Estimated from measured bridge frequency, **: Second resonance, ***: Third resonance.

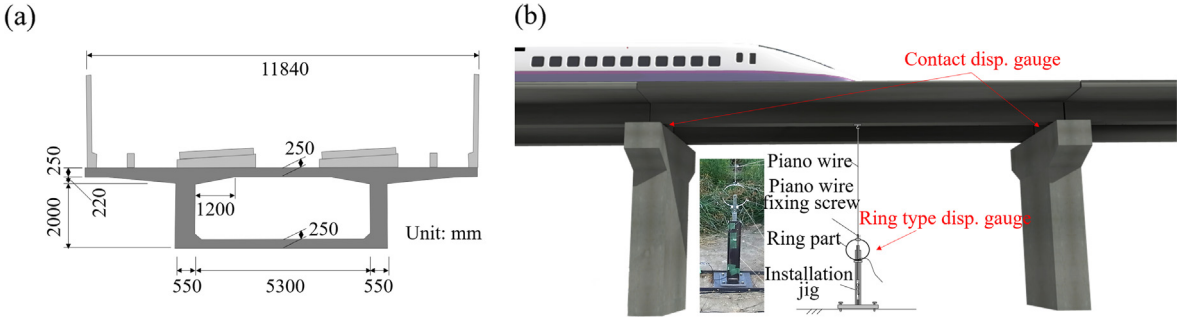


Fig. 19. (a) Sectional view of a target bridge and (b) example of a displacement measurement (Bridge #1).

5.3. Results of the first-resonance bridge

Fig. 20 shows the input displacement responses, instantaneous natural frequencies, and instantaneous modal damping ratios of Bridge #1. The natural frequency and modal damping ratio of the bridge alone (without the VBI effect) were identified from the responses after the train passage, and they are denoted as “free vibration” in Fig. 20. Fig. 21 shows the instantaneous power spectrum obtained from the estimation results. The input response shows a clear resonance phenomenon, in which the amplitude increases during the train passage. The estimated time-varying coefficients $\hat{\beta}_m$ (blue lines in the plots) varied under the modal external force action (Fig. 20 (b) and (c)). During the train passage, the instantaneous natural frequency calculated from the time-varying coefficients $\hat{\beta}_m$ decreased by approximately 0.05 Hz, and the instantaneous modal damping ratio increased by approximately 1% (Fig. 20(d) and (e)). These variations are reflected in the instantaneous power spectrum (Fig. 21). Also during the train passage, the spectral peak shifted to the lower frequency side, and its magnitude decreased with increasing modal damping ratio.

5.4. Accuracy of the VBI effect obtained by the VBI model

Fig. 20 also shows the result based on displacement response simulated by the VBI model (labeled VBI-TVARX in the figs). The instantaneous natural frequency and modal damping ratio in the VBI model show the same tendencies as the measured values (labeled Exp.-TVARX). This result implies that the assumption holds such as few rail irregularities and no spatial stiff-

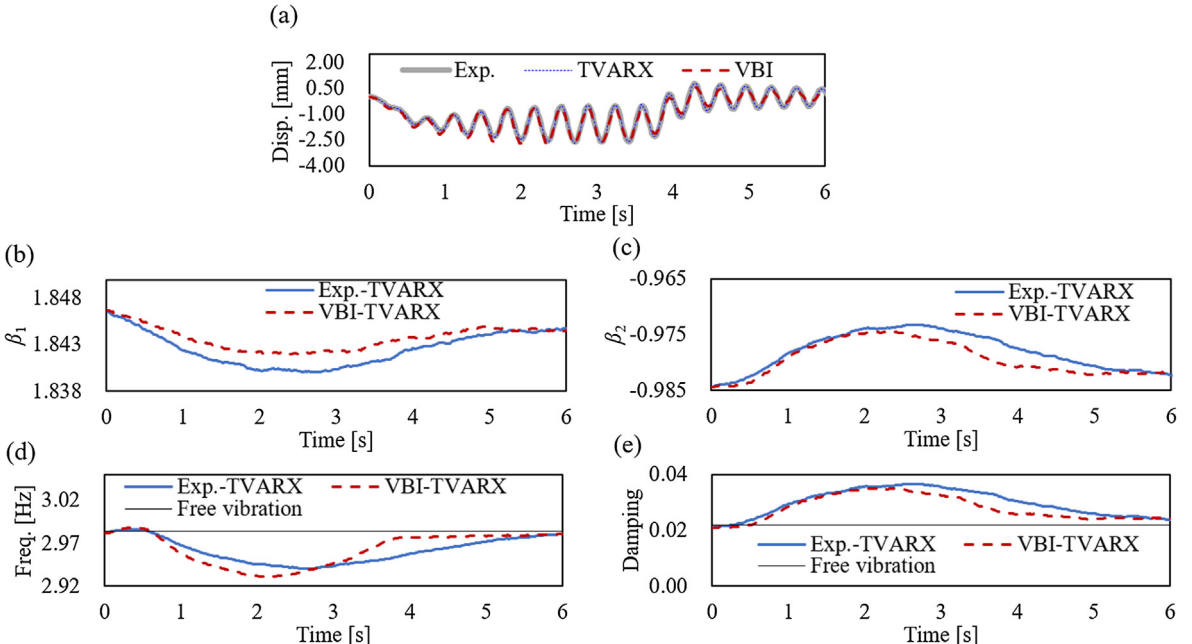


Fig. 20. Measured and VBI-simulated displacement responses of Bridge #1; (a) displacement responses, (b) time-varying coefficient β_1 , (c) time-varying coefficient β_2 , (d) natural frequency, and (e) modal damping ratio.

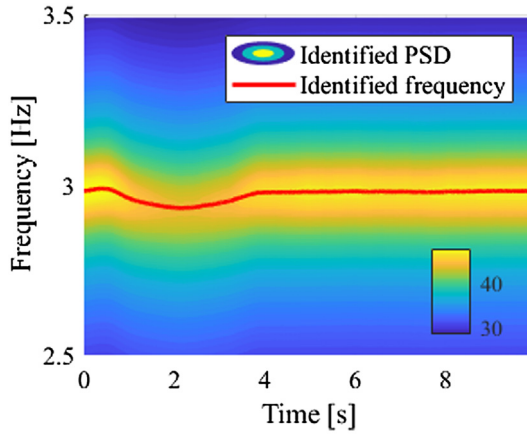


Fig. 21. Instantaneous power spectrum of Bridge #1 estimated by the TVARX model.

ness parameter changes in the target bridge. In addition, the displacement response simulated by the VBI model includes the VBI effect (i.e., the decreased instantaneous natural frequency and increased instantaneous modal damping ratio), as observed on actual bridges.

5.5. Results of other first-resonance bridges

Fig. 22 shows the first-resonance responses of two other railway bridges. On both bridges, the instantaneous natural frequency decreased, and the instantaneous modal damping ratio increased during the train passage, confirming that these phenomena inherently result from the train passage and are not irregular fluctuations. In the numerical example (Fig. 9), the instantaneous natural frequency and modal damping ratio varied at each timing of the passing vehicle. Such variations, which were not observed in the field measurements, correspond to the passage of the entire train composed of multiple vehicles. This might be caused by the long-span length of the target bridges. As the train crossed the long-span bridge, the variations became smoother with the increase in the number of wheelsets present on the bridge.

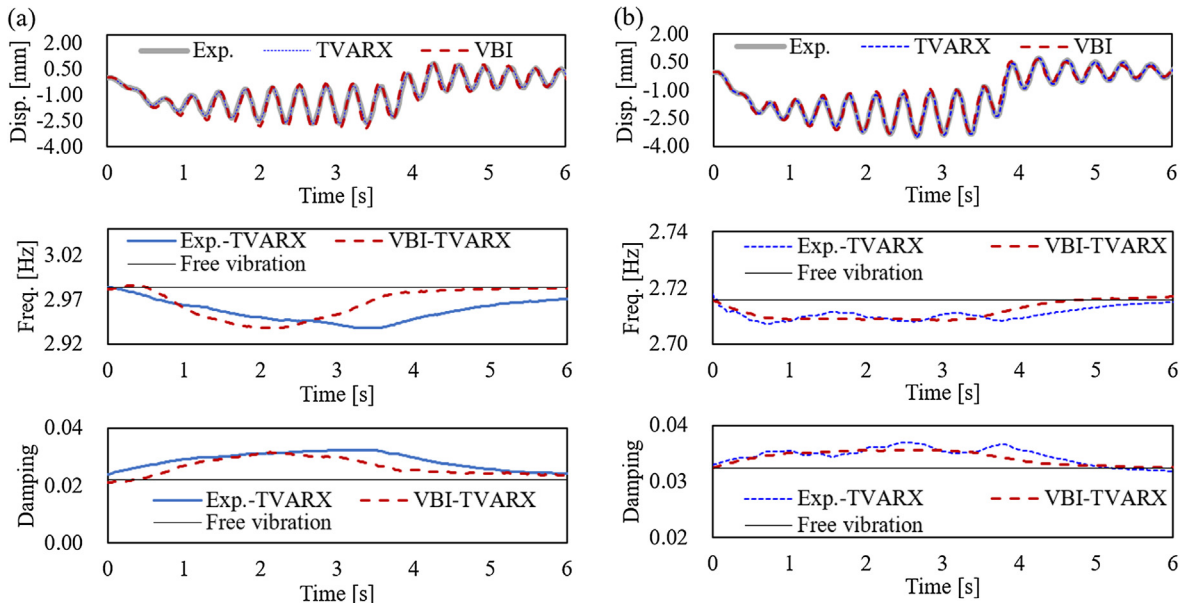


Fig. 22. (Top to bottom): Measured and VBI-simulated displacement responses, instantaneous natural frequencies, and instantaneous modal damping ratios of (a) Bridge # 2 and (b) Bridge #3.

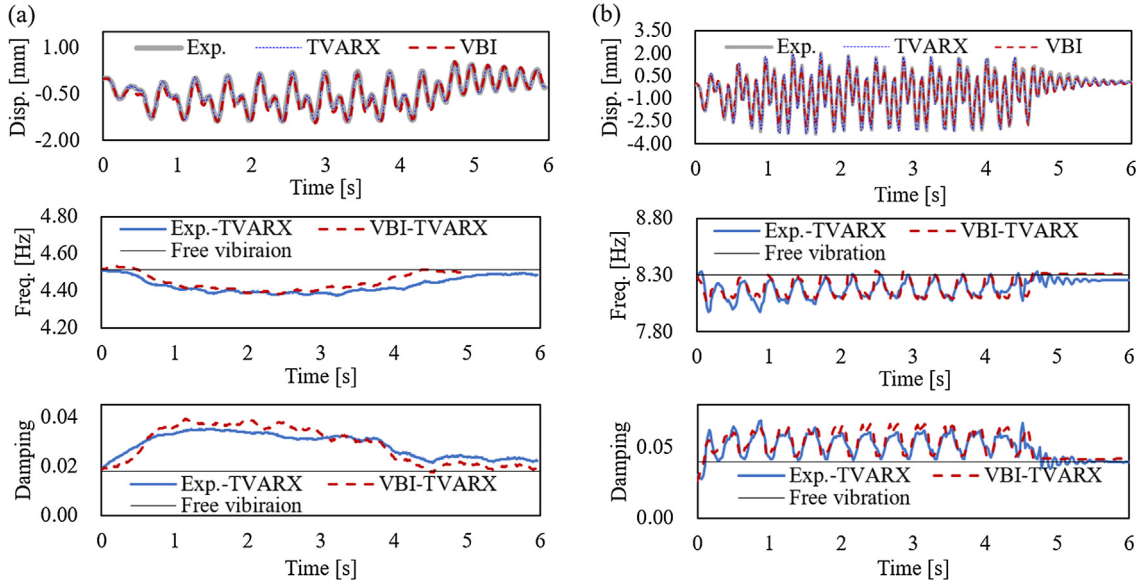


Fig. 23. (Top to bottom): Measured and VBI-simulated displacement responses, instantaneous natural frequencies, and instantaneous modal damping ratios of (a) Bridge #4 with second resonance and (b) Bridge #5 with third resonance.

5.6. Results of second and third resonance bridges

Fig. 23 shows the displacement responses during the second and third resonances. These resonances occur when each vehicle passes at the timing of two or three natural waves of the bridge. During the train passage, the instantaneous natural frequency and modal damping ratio decreased and increased, respectively, over the whole train length on Bridge #4 (with second resonance), but decreased and increased, respectively, with the passage of each vehicle on Bridge #5 (with third resonance). The third resonance on Bridge #5 occurred at a span length of 9.3 m, shorter than the bogie interval (15 m). Therefore, during the train passage, no wheelset exists on the bridge at certain times. The instantaneous natural frequency and modal damping ratio at these timings coincided with the natural frequency and the modal damping ratio of the bridge itself, without the VBI effect. This result supports that no VBI effect occurs when there is no wheelset on the bridge. The VBI effects at high order resonances appear to be rarely reported and are clarified at the second and third resonances for the first time in the present study.

As demonstrated in the above results, the proposed method estimates the apparent variations in the natural frequency and modal damping ratio caused by the VBI effect in the measured displacement response. This result enables researchers to use VBI model simulation in order to investigate the factors with strong impact on the VBI effect. The VBI effect of traveling vehicles on the bridge and its generation mechanism were also analyzed by the VBI model and the proposed method.

6. Conclusions

This study proposed a novel method that estimates the VBI effect of a train passing over a bridge. The VBI effect causes a temporal variation of the bridge's natural frequency and modal damping. After the validation of the algorithm with a numerical calculation, the proposed method was applied to measured responses of the actual bridges. The main results are summarized below.

- 1) The novel hierarchical Bayesian estimation method of the TVARX model simultaneously considers the train load (as a modal external force) and the temporal variation of the system parameters. The proposed method estimates the time-varying natural frequency and modal damping ratio under the VBI effect from the forced vibration state during the train passage.
- 2) The proposed method accurately captured the calculated variations in the natural frequency and modal damping ratio during the train passage. These variations cannot be estimated by previous time-frequency analysis methods such as the TVVAR model.
- 3) The proposed method is applied to the VBI simulation results of various train speeds and rail irregularities. Therefore, if the train speed is within $\pm 10\%$ of the resonance speed, the instantaneous natural frequency and instantaneous modal damping ratio can be accurately estimated. The effect of rail irregularity only appears in the instantaneous natural frequency at the time in which the first and second vehicles pass. Although the effect becomes small after the passage of the third vehicle, the rail irregularity effect on the instantaneous modal damping ratio is limited.

- 4) The proposed method is applied to the resonance responses measured on real bridges, and it is demonstrated that the fluctuation of the instantaneous natural frequency and the instantaneous modal damping ratio can be estimated. Moreover, the reliability of the obtained results was verified based on a comparison with VBI simulation.

Despite the achievements of this research, several limitations remain.

In SHM, in addition to the VBI effect, the non-linearity due to crack damage is predicted to affect the instantaneous natural frequency and instantaneous modal damping ratio. It is important to construct and verify the method to estimate the non-linearity because of the physical parameters of the bridge along with the VBI effect. It is considered that a part of this task can be achieved by combining the proposed method and VBI simulation. The authors are confirming that applying the TVARX model to a real bridge with breathing cracks can identify instantaneous and amplitude-dependent changes in stiffness (natural frequency). The details will be reported in another opportunity that follows in this study.

The variations in natural frequency and modal damping ratio were modeled by a random walk process in this study. However, in the obtained results, these temporal variations appeared as approximate functions of the modal external force. Therefore, by modeling the temporal variations of the natural frequency and modal damping ratio as a functional form based on the modal external force, we could limit the estimation parameters. In addition, the generation mechanism of the VBI effect likely depends on the natural-frequency relationships between the bridge and each part of the vehicle [9]. In a future work, the VBI effect will be further verified under various conditions.

Acknowledgment

This study was conducted as a general study of the organization (RTRI) to which First Author belongs. Therefore, there is no financial assistance from the other organizations and funders.

Appendix I List of symbols

Table 5. 1 shows the list of symbols used in this study.

Table 5

List of symbols.

Symbols	Description
L	Bridge span length
$m/c/El$	Unit-length mass/damping coefficient/bending stiffness of bridge
$y_{x,t}$	Bridge vertical response at position x and time point t
x	Horizontal position where the left end of the bridge is 0
i/nw	Wheelset number/maximum wheelset number
P_s	Stationary wheel load
P_d	Dynamically time-varying component in the wheel load
δ	Dirac delta function
v	Train traveling velocity
τ_i	Distance from the left end of the beam to the i th wheelset at the initial time point
$z_{c,t}$	Car body vertical displacement
$\psi_{c,t}$	Car body pitching rotation
$z_{1,t}/z_{2,t}$	Front/rear bogie vertical displacement
$\psi_{1,t}/\psi_{2,t}$	Front/rear bogie pitching rotation
$z_{ti,t}$	Bogie vertical displacement at the position just above i th wheelset
$m_c/m_t/m_w$	Car body/bogie/wheelset mass
J_c/J_t	Car body/bogie rotational inertia
c_s/k_s	Viscous damping/spring coefficient of secondary suspensions
c_p/k_p	Viscous damping/spring coefficient of primary suspensions
c_{cs}/k_{cs}	Viscous damping/spring coefficient of car body connector
$b/r/L_v$	Distances between the wheelsets on a bogie/the bogie centers on a vehicle/the vehicle length
$Ir(x)$	Rail irregularity at position x
$\Phi_{n,x}/z_{n,t}/n$	Modal shape vector/modal displacement/modal number of bridge; $1, \dots, N$
$m_b/c_b/k_b$	Modal mass/damping/stiffness of bridge
$A_{i,t}$	Modal shape function of bridge
H	Heaviside unit function
f/ξ	Natural frequency/modal damping ratio of bridge
m/Δ	Discrete time point; $1, \dots, M$ /time interval
\mathbf{A}_m	Bridge modal function vector corresponding to each wheelset; $[A_{1,m-1}, \dots, A_{nw,m-1}]^T$
$\boldsymbol{\alpha}$	Regression coefficient vector of modal function; $[\alpha_1, \dots, \alpha_{nw}]^T$
\mathbf{Z}_m	Explanatory variable vector of autocorrelation; $[z_{m-1}, z_{m-2}]$
β	Autocorrelation coefficient vector; $[\beta_1, \beta_2]^T$
ϵ_m	

(continued on next page)

Table 5 (continued)

Symbols	Description
σ_ϵ^2	Observation noise; $\epsilon_m \sim N(0, \sigma_\epsilon^2)$
α_i	Variance of observation error distribution
$P_{i,S}$	Modified stationary wheel load on AR model; $P_{i,S}/\gamma$
γ	Correction factor for central difference discretization; $\frac{m_b}{\Delta^2} + \frac{c_b}{2\Delta}$
$\Delta m_v/\Delta c_v/\Delta k_v$	Additional components of the vehicle mass/damping/stiffness to the bridge modal mass/damping/stiffness resulting from the vehicle response and track irregularities associated with the bridge response
$\hat{P}_{i,D}$	Dynamically time-varying component in the wheel load excluding the component related to the bridge response
f_t/ξ_t	Time-varying natural frequency/modal damping ratio
f_m/ξ_m	Instantaneous natural frequency/modal damping ratio at time point m
$\kappa_t^m/\kappa_t^c/\kappa_t^k$	Mass/damping/stiffness ratio between bridge and some parts of vehicle corresponding to the VBI
β_m	Time-varying autocorrelation coefficient vector; $\beta_m = [\beta_{1,m}, \beta_{2,m}]^T$
γ_m	Correction factor for central difference discretization; $\gamma_m = (1 + \kappa_{m-1}^m) \frac{m_b}{\Delta^2} + (1 + \kappa_{m-1}^c) \frac{c_b}{2\Delta}$
\mathbf{v}_m	Stride of random walk with time-varying coefficient β_m ; $\mathbf{v}_m \sim N(0, \Sigma_v)$
Σ_v	Variance-covariance matrix of random walk stride
β_0	Initial autocorrelation coefficient vector
Σ_β	Variance-covariance matrix of autocorrelation coefficients PDF
$\lambda/\tilde{\lambda}$	System pole variable/pole of the system that satisfies $ \lambda^2 + \lambda\beta_{1,m} + \beta_{2,m} = 0$
$PS_{f,m}$	Time-varying power spectral density
θ	Unknown parameter vector to be estimated; $\theta = [\beta_1, \dots, \beta_M, \sigma_\epsilon, \Sigma_v, \alpha]$
$\tilde{\mathbf{z}}$	Observation value vector; $\tilde{\mathbf{z}} = [\tilde{z}_1, \dots, \tilde{z}_M]$
$\pi(\theta)/\pi(\theta \tilde{\mathbf{z}})$	Prior/posterior PDF
$L(\tilde{\mathbf{z}} \theta)$	likelihood function
$\pi(\sigma_\epsilon)$	Prior PDF of σ_ϵ ($= IW(\sigma_{e0}^2, v_{e0}, M)$)
$\pi(\alpha)$	Prior PDF of α (unconditional prior PDF with uniform probability density)
$\pi(\Sigma_v)$	Prior PDF of Σ_v ($= IW(\Sigma_{v0}, v_{v0}, M - 1)$)
$\pi(\beta_{m+1} \beta_m, \Sigma_v)$	Prior PDF of β_{m+1} ($= N(\beta_m, \Sigma_v)$)
$N()$	Multivariate-normal distribution
$IW()$	Inverse-Wishart distribution
\mathbf{B}	Time-varying autocorrelation coefficient matrix; $\mathbf{B} = [\beta_1, \dots, \beta_M]$
Λ	Explanatory variable matrix of exogenous variable; $\Lambda = [A_1^T, \dots, A_{M-1}^T]$
\mathbf{Z}_x	Modified observed value vector for exogenous variable estimation; $\mathbf{Z}_x = [\tilde{z}_2 - \mathbf{Z}_2 \beta_2, \dots, \tilde{z}_M - \mathbf{Z}_M \beta_M]$
$\pi(\mathbf{B}, \mathbf{z})$	Joint occurrence probability of variable \mathbf{B} and \mathbf{z}
$E(\mathbf{B}, \mathbf{z})$	Expected value of Joint occurrence probability of variable \mathbf{B} and \mathbf{z}
$\hat{\mathbf{B}} = E(\mathbf{B} \mathbf{z})$	Expected value of probability of variable \mathbf{B} of conditional \mathbf{z}
F_m	$F_m = \mathbf{Z}_m \Sigma_{\beta,m} \mathbf{Z}_m^T + \sigma_\epsilon^2$ for DK smoother
\mathbf{K}_m	$\mathbf{K}_m = \Sigma_{\beta,m} \mathbf{Z}_m^T F_m^{-1}$ for DK smoother
\mathbf{L}_m	$\mathbf{L}_m = \mathbf{E} - \mathbf{K}_m \mathbf{Z}_m$ for DK smoother
\mathbf{r}_{m-1}	$\mathbf{r}_{m-1} = \mathbf{Z}_m F_m \mathbf{v}_m + \mathbf{L}_m^T \mathbf{r}_m$ for DK smoother
\mathbf{E}	Unit matrix
$n_g/\bar{n}/n$	Number of iterations/burn-in/maximum iterations in MCMC calculation
AE_f/n_{train}	Average error index/Number of samples during train passing
$S_{rr}(\Omega)$	One-sided power spectral density function of rail irregularities; $S_{rr}(\Omega) = kA \frac{\Omega^2}{(\Omega^2 + \Omega_c^2)\Omega}$
$\Omega/k/\Omega_c$	Wave number ($2\pi/L_r$)/0.25/0.8245
L_r	Wave length of rail irregularities

Appendix II Vehicle–bridge dynamic interaction (VBI) model

This appendix derives the motion equations of the VBI model shown in Fig. 3. The responses of the railway bridges and a train crossing at constant speed v [m/s] were modeled on a two-dimensional vehicle model with 6 degrees of freedom per vehicle and a railway bridge model with a two-dimensional simply supported beam. Similar modeling has been studied in many previous studies [4,9,37], so is only outlined here. The degrees of freedom of the bridge and vehicle are defined as row vectors $\mathbf{Z}_{N,t} = [z_{1,t}, \dots, z_{N,t}]^T$ and $\mathbf{Z}_{c,t} = [z_{c,t}, \psi_{c,t}, z_{t1,t}, \psi_{t1,t}, z_{t2,t}, \psi_{t2,t}]^T$, respectively. Let the wheelset freedoms $\mathbf{Z}_{w,t}$ that is equal to the bridge displacement $\mathbf{Z}_{N,t}\mathbf{A}$ add the rail irregularity \mathbf{Ir} at the axle position as follows:

$$\mathbf{Z}_{w,t} = \mathbf{Z}_{N,t}\mathbf{A} + \mathbf{Ir} \quad (I.1)$$

Considering the dynamic variation component $P_{i,D}$ of the wheel load as a coupling term with the vehicle model in Fig. 3, we obtain

$$\begin{aligned} & \left[\begin{array}{c} \mathbf{M}_b^* \\ \mathbf{M}_c \end{array} \right] \left[\begin{array}{c} \ddot{\mathbf{Z}}_{N,t} \\ \ddot{\mathbf{Z}}_{c,t} \end{array} \right] + \left[\begin{array}{cc} \mathbf{C}_b^* & \mathbf{C}_{b,c} \\ \mathbf{C}_{c,b} & \mathbf{C}_c \end{array} \right] \left[\begin{array}{c} \dot{\mathbf{Z}}_{N,t} \\ \dot{\mathbf{Z}}_{c,t} \end{array} \right] + \left[\begin{array}{cc} \mathbf{K}_b^* & \mathbf{K}_{b,c} \\ \mathbf{K}_{c,b} & \mathbf{K}_c \end{array} \right] \left[\begin{array}{c} \mathbf{Z}_{N,t} \\ \mathbf{Z}_{c,t} \end{array} \right] \\ &= \left[\begin{array}{c} \mathbf{A}^T (\mathbf{F}_{gw} - \mathbf{K}_{wt} \mathbf{K}_{tt}^{-1} \mathbf{F}_{gt}) \\ 0 \end{array} \right] - \nu^2 \left[\begin{array}{c} \mathbf{A}^T \mathbf{M}_{ww} \\ 0 \end{array} \right] \mathbf{I}r - \nu \left[\begin{array}{c} \mathbf{A}^T \mathbf{C}_{ww} \\ -\mathbf{C}_{tw} \end{array} \right] \mathbf{I}r - \left[\begin{array}{c} \mathbf{A}^T \mathbf{K}_{ww} \\ -\mathbf{K}_{tw} \end{array} \right] \mathbf{I}r \end{aligned} \quad (I.2)$$

where

$$\mathbf{M}_b^* = \mathbf{M}_b + \mathbf{A}^T \mathbf{M}_w \mathbf{A} \quad (I.3)$$

$$\mathbf{C}_b^* = \mathbf{C}_b + \mathbf{A}^T \mathbf{C}_w \mathbf{A}, \quad (I.4)$$

$$\mathbf{K}_b^* = \mathbf{K}_b + \mathbf{A}^T \mathbf{K}_w \mathbf{A} \quad (I.5)$$

$$\mathbf{A}(i, n) = \sin \left\{ \frac{n\pi(\nu t - \tau_i)}{L} \right\} \left\{ H\left(t - \frac{\tau_i}{\nu}\right) - H\left(t - \frac{\tau_i + L}{\nu}\right) \right\}$$

$$\text{with } (i = 1, \dots, nw), (n = 1, \dots, N) \quad (I.6)$$

\mathbf{M}_b , \mathbf{C}_b , and \mathbf{K}_b are the mass, damping, and rigidity matrices in the modal coordinates of the bridge, respectively. These matrices are expressed as follows:

$$\mathbf{M}_b = \text{Diag}(m_{b1}, \dots, m_{bN}) = \text{Diag}(\bar{m}L/2, \dots, \bar{m}L/2), \quad (I.7)$$

$$\mathbf{C}_b = \text{Diag}(c_{b1}, \dots, c_{bN}) = \text{Diag}(2\xi_1 \sqrt{m_{b1}, k_{b1}}, \dots, 2\xi_N \sqrt{m_{bN}, k_{bN}}), \quad (I.8)$$

$$\mathbf{K}_b = \text{Diag}(k_{b1}, \dots, k_{bN}) = \text{Diag}((2\pi f_1)^2 m_b, \dots, (2\pi N^2 f_N)^2 m_b). \quad (I.9)$$

\mathbf{M}_c , \mathbf{C}_c , and \mathbf{K}_c are the mass, damping, and rigidity matrices of the vehicle, respectively; \mathbf{M}_w , \mathbf{C}_w , and \mathbf{K}_w are the mass, damping, and rigidity matrices of the wheelsets, respectively; and $\mathbf{C}_{b,c}$ ($\mathbf{C}_{c,b} = \mathbf{C}_{b,c}^T$) and $\mathbf{K}_{b,c}$ ($\mathbf{K}_{c,b} = \mathbf{K}_{b,c}^T$) are the coupling terms related to the vehicle dampers and springs, respectively:

$$\mathbf{M}_c = \text{Diag}(m_c, J_c, m_t, J_t, m_t, J_t) \quad (I.10)$$

$$\mathbf{C}_c = \begin{bmatrix} 2c_s & 0 & -c_s & 0 & -c_s & 0 \\ & \frac{c_s L_c^2}{2} & \frac{c_s L_c}{2} & 0 & -\frac{c_s L_c}{2} & 0 \\ & & c_s + 2c_p & 0 & 0 & 0 \\ & & & \frac{c_p b^2}{2} & 0 & 0 \\ & Sym. & & & c_s + 2c_p & 0 \\ & & & & & \frac{c_p b^2}{2} \end{bmatrix}, \quad (I.11)$$

$$\mathbf{K}_c = \begin{bmatrix} 2k_s & 0 & -k_s & 0 & -k_s & 0 \\ & \frac{k_s L_c^2}{2} & 0 & -\frac{k_s L_c}{2} & 0 & 0 \\ & & k_s + 2k_p & 0 & 0 & 0 \\ & & & \frac{k_p b^2}{2} & 0 & 0 \\ & Sym. & & & k_s + 2k_p & 0 \\ & & & & & \frac{k_p b^2}{2} \end{bmatrix}, \quad (I.12)$$

$$\mathbf{M}_w = \text{diag}(m_w, m_w, m_w, m_w), \quad (I.13)$$

$$\mathbf{C}_w = \text{diag}(c_p, c_p, c_p, c_p) \quad (I.14)$$

$$\mathbf{K}_w = \text{diag}(k_p, k_p, k_p, k_p) \quad (I.15)$$

$$\mathbf{C}_{b,c} = \begin{bmatrix} 0 & 0 & -c_p & -\frac{c_p b}{2} & 0 & 0 \\ 0 & 0 & -c_p & -\frac{c_p b}{2} & 0 & 0 \\ 0 & 0 & 0 & 0 & -c_p & -\frac{c_p b}{2} \\ 0 & 0 & 0 & 0 & -c_p & -\frac{c_p b}{2} \end{bmatrix} \quad (\text{I.16})$$

$$\mathbf{K}_{b,c} = \begin{bmatrix} 0 & 0 & -k_p & -\frac{k_p b}{2} & 0 & 0 \\ 0 & 0 & -k_p & -\frac{k_p b}{2} & 0 & 0 \\ 0 & 0 & 0 & 0 & -k_p & -\frac{k_p b}{2} \\ 0 & 0 & 0 & 0 & -k_p & -\frac{k_p b}{2} \end{bmatrix} \quad (\text{I.17})$$

The vehicles are coupled through the vertical spring k_{cs} and the damper c_{cs} . These components are introduced into the coupling term of the vertical displacement and the rotational degrees of freedom of the car bodies of two adjacent vehicles (when the vehicle model contains two or more cars).

The VBI model (I.2) was solved and modeled in state space. The numerical integration was performed by the explicit Runge–Kutta method (4, 5) proposed by Dormand and Prince (also known as RK5(4)7FM, DOPRI5, and DP(4, 5) [72]). The present VBI model simulation considers bridge modes 1–5 (i.e., $N = 5$) [4].

Appendix III Prior and conditional posterior PDF of the TVARX model

The prior PDFs $\pi(\theta)$ corresponding to the unknown parameters $\theta = [\beta_1, \dots, \beta_M, \sigma_\epsilon, \Sigma_v, \alpha]$ are given by

$$\pi(\beta_{m+1}) = N(\beta_m, \Sigma_v), \quad (m = 1, \dots, M-1), \quad (\text{II.1})$$

$$\pi(\beta_1) = N(\beta_0, \Sigma_{\beta 0}) \quad (\text{II.2})$$

$$\pi(\sigma_\epsilon^2) = IW(\sigma_{\epsilon 0}^2, v_{\epsilon 0}, M), \quad (\text{II.3})$$

$$\pi(\Sigma_v) = IW(\Sigma_{v0}, v_{v0}, M-1) \quad (\text{II.4})$$

where IW is the reciprocal distribution of the Wishart distribution W . The M_0 random variables follow the PDF of the Wishart distribution with v_0 degrees of freedom and variance–covariance matrix Σ_0 [39]:

$$W(\Sigma^{-1} | \Sigma_0, v_0, M_0) = \Psi^{-1} |\Sigma|^{\frac{v_0 - M_0 - 1}{2}} \exp \left\{ \frac{\text{Tr}(\Sigma_0^{-1} \Sigma^{-1})}{2} \right\} \quad (\text{II.5})$$

where

$$\Psi = 2^{\frac{M_0 v_0}{2}} \pi^{\frac{M_0(M_0-1)}{2}} |\Sigma_0|^{\frac{M_0}{2}} \prod_{m_0=1}^{M_0} \Gamma \left(\frac{v_0 - m_0 + 1}{2} \right) \quad (\text{II.6})$$

$\text{Tr}(\cdot)$ in Eq. (II.5) indicates the trace of the matrix, and $\Gamma(\cdot)$ in Eq. (II.6) denotes the gamma function.

β_1 is drawn from the conditional posterior PDF $\pi(\beta_1 | \mathbf{B}_{-1}, \sigma_\epsilon, \Sigma_v, \alpha, \tilde{\mathbf{z}})$ given by $\beta_1 \sim N(\beta_{\beta 1}, \Sigma_{\beta 1})$, with $\beta_{\beta 1}$ and $\Sigma_{\beta 1}$ expressed as follows:

$$\beta_{\beta 1} = \Sigma_{\beta 1} \left(\Sigma_{\beta 0}^{-1} \beta_0 + \frac{\mathbf{Z}^T \mathbf{Z}_\beta}{\sigma_\epsilon^2} \right), \quad (\text{II.7})$$

$$\Sigma_{\beta 1}^{-1} = \Sigma_{\beta 0}^{-1} + \mathbf{Z}^T \mathbf{Z} / \sigma_\epsilon^2 \quad (\text{II.8})$$

$$\mathbf{Z} = \begin{bmatrix} \tilde{z}_2, \dots, \tilde{z}_{m-1}, \dots, \tilde{z}_{M-1} \\ \tilde{z}_1, \dots, \tilde{z}_{m-2}, \dots, \tilde{z}_{M-2} \end{bmatrix}^T \quad (\text{II.9})$$

$$\mathbf{Z}_\beta = \begin{bmatrix} \tilde{z}_1 - \mathbf{A}_1 \alpha - \mathbf{Z}_1 \beta_1, \dots, \tilde{z}_M - \mathbf{A}_M \alpha - \mathbf{Z}_M \beta_M \end{bmatrix} \quad (\text{II.10})$$

σ_ϵ is drawn from the conditional posterior PDF $\pi(\sigma_\epsilon | \mathbf{B}, \Sigma_v, \alpha, \tilde{\mathbf{z}})$ given by $\sigma_\epsilon^2 \sim IW(\sigma_{\epsilon 1}^2, v_{\epsilon 1}, M)$, with $\sigma_{\epsilon 1}^2$ and $v_{\epsilon 1}$ expressed as follows:

$$\sigma_{\epsilon 1}^2 = \sigma_{\epsilon 0}^2 + \sum_{m=1}^M \left(\tilde{z}_m - \mathbf{A}_m \boldsymbol{\alpha} + \mathbf{Z}_m \boldsymbol{\beta}_m \right)^2 \quad (\text{II.11})$$

$$v_{\epsilon 1} = v_{\epsilon 0} + M \quad (\text{II.12})$$

Σ_v is drawn from the conditional posterior PDF $\pi(\Sigma_v | \mathbf{B}, \sigma_\epsilon, \boldsymbol{\alpha}, \tilde{\mathbf{z}})$ given by $\Sigma_v \sim IW(\Sigma_{v1}, v_{v1}, M - 1)$, with Σ_{v1} and v_{v1} expressed as follows:

$$\Sigma_{v1} = \Sigma_{v0} + \sum_{m=1}^{M-1} (\boldsymbol{\beta}_{m+1} - \boldsymbol{\beta}_m)(\boldsymbol{\beta}_{m+1} - \boldsymbol{\beta}_m)^T \quad (\text{II.13})$$

$$v_{v1} = v_{v0} + M. \quad (\text{II.14})$$

Appendix IV Independence of variance in conditional probability [46]

This appendix discusses the statistical properties of the variance [45] in the conditional probability, which is the basic principle of the DK smoother. Let us consider drawing arbitrary vectors \mathbf{P} and \mathbf{Q} from the conditional PDF $\pi(\mathbf{P}|\mathbf{Q})$, and both \mathbf{P} and \mathbf{Q} follow simultaneous linear normal distributions with PDF $\pi(\mathbf{P}, \mathbf{Q})$. Denote the samples following PDF $\pi(\mathbf{P}, \mathbf{Q})$ as vectors \mathbf{P}^+ and \mathbf{Q}^+ . Assuming the expected value and variance of the conditional PDF $\pi(\mathbf{P}|\mathbf{Q})$ as $\hat{\mathbf{P}} = E(\mathbf{P}|\mathbf{Q})$ and $W = \text{var}(\mathbf{P}|\mathbf{Q})$, respectively, the variance W does not depend on \mathbf{Q} . Therefore, if $\hat{\mathbf{P}}^+ = E(\mathbf{P}^+|\mathbf{Q}^+)$ is the expected value of the conditional PDF of \mathbf{Q}^+ for sample \mathbf{P}^+ following PDF $\pi(\mathbf{P}, \mathbf{Q})$, then $\mathbf{P}^0 = \hat{\mathbf{P}} + \mathbf{P}^+ - \hat{\mathbf{P}}^+$ is sampled from the conditional PDF $\pi(\mathbf{P}|\mathbf{Q})$ [50]. When samples are not easily drawn directly from the conditional PDF $\pi(\mathbf{P}|\mathbf{Q})$, they can be drawn from the simultaneous PDF $\pi(\mathbf{P}, \mathbf{Q})$. The expected values $E(\mathbf{P}|\mathbf{Q})$ and $E(\mathbf{P}^+|\mathbf{Q}^+)$ are then equivalent to drawing from the conditional PDF $\pi(\mathbf{P}|\mathbf{Q})$. Replacing this approach with the drawing of the time-varying coefficient, one obtains the DK smoother developed in subsection 2.7.

References

- [1] L. Fryba, Vibration of Solids and Structures Under Moving Loads, Springer Science & Business Media, 2013.
- [2] Y.B. Yang, J.D. Yau, L.C. Hsu, Vibration of simple beams due to trains moving at high speeds, Eng. Struct. 19 (1997) 936–944.
- [3] M. Sogabe, N. Matsumoto, M. Kanamori, H. Wakui, Impact factors of concrete girders coping with train speed-up, Quart. Rep. RTRI 46 (2005) 46–52.
- [4] A. Matsuura, Dynamic behavior of bridge girder for high speed railway bridge, Quart. Rep. RTRI (1979) 70–76.
- [5] M. Sogabe et al., Impact factors of concrete girders coping with train speed-up, Quart. Rep. RTRI 46 (2005) 46–52.
- [6] M. Sogabe et al., Deflection limits of structures for train speed-up, Quart. Rep. RTRI 46 (2005) 130–136.
- [7] British Standard Institution. Eurocode 1: Actions on structures. Traffic Loads on Bridges. 2005. BSI.
- [8] K. Liu, G. de Roeck, G. Lombaert, The effect of dynamic train–bridge interaction on the bridge response during a train passage, J. Sound. Vib. 325 (2009) 240–251.
- [9] A. Doménech, P. Museros, M.D. Martínez-Rodrigo, Influence of the vehicle model on the prediction of the maximum bending response of simply-supported bridges under high-speed railway traffic, Eng. Struct. 72 (2014) 123–139.
- [10] Xu, Lei, Wanming Zhai, A three-dimensional model for train-track-bridge dynamic interactions with hypothesis of wheel-rail rigid contact, Mech. Syst. Sig. Process. 132 (2019) 471–489.
- [11] D. Feng, H. Sun, M.Q. Feng, Simultaneous identification of bridge structural parameters and vehicle loads, Comput. Struct. 157 (2015) 76–88.
- [12] A. Cury, C. Cremona, Assignment of structural behaviours in long-term monitoring: application to a strengthened railway bridge, Struct. Health Monit. 11 (2012) 422–441.
- [13] D. Ribeiro, R. Calçada, R. Delagado, M. Brehm, V. Zabel, Finite element model updating of a bowstring-arch railway bridge based on experimental modal parameters, Eng. Struct. 40 (2012) 413–435.
- [14] O.S. Salawu, Detection of structural damage through changes in frequency: a review, Eng. Struct. 19 (1997) 718–723.
- [15] K. Matsuoka, K. Kaito, M. Tokunaga, T. Watanabe, M. Sogabe, Estimation of bridge deflection response under passing train loads based on acceleration, Jpn. Soc. Civ. Eng. Ser. A1 (Struct. Eng. Earthq. Eng. (SE/EE)) 69 (2013) 527–542 (In Japanese).
- [16] L. Garibaldi, S. Fassòis, MSSP special issue on the identification of time varying structures and systems, Mech. Syst. Signal Process. 1 (2014) 1–2.
- [17] Z.S. Ma, L. Liu, S.D. Zhou, L. Yu, F. Naets, W. Heylen, W. Desmet, Parametric output-only identification of time-varying structures using a kernel recursive extended least squares TARMA approach, Mech. Syst. Signal Process. 98 (2018) 684–701.
- [18] J.K. Hammond, P.R. White, The analysis of non-stationary signals using time-frequency methods, J. Sound Vib. 190 (1996) 419–447.
- [19] Y. Guo, A. Kareem, Non-stationary frequency domain system identification using time-frequency representations, Mech. Syst. Signal Process. 72 (2016) 712–726.
- [20] L. Cohen, Time-frequency analysis, Vol. 778, Prentice hall, 1995.
- [21] P. Bonato, R. Ceravolo, A. De Stefano, F. Molinari, Use of cross-time-frequency estimators for structural identification in non-stationary conditions and under unknown excitation, J. Sound Vib. 237 (2000) 775–791.
- [22] S.D. Zhou, W. Heylen, P. Sas, L. Liu, Parametric modal identification of time-varying structures and the validation approach of modal parameters, Mech. Syst. Signal Process. 47 (2014) 94–119.
- [23] R. Ghanem, F. Romeo, A wavelet-based approach for the identification of linear time-varying dynamical systems, J. Sound Vib. 234 (2000) 555–576.
- [24] W.J. Staszewski, D.M. Wallace, Wavelet-based frequency response function for time-variant systems—an exploratory study, Mech. Syst. Signal Process. 47 (2014) 35–49.
- [25] D. Hester, A. González, A wavelet-based damage detection algorithm based on bridge acceleration response to a vehicle, Mech. Syst. Signal Process. 28 (2012) 145–166.
- [26] D. Cantero, M. Ülker-Kaustell, R. Karoumi, Time-frequency analysis of railway bridge response in forced vibration, Mech. Syst. Signal Process. 76 (2016) 518–530.
- [27] M. Feldman, Time-varying vibration decomposition and analysis based on the Hilbert transform, J. Sound Vib. 295 (2006) 518–530.

- [28] E.S. Carbajo, R.S. Carbajo, C. Mc Goldrick, B. Basu, ASDAH: An automated structural change detection algorithm based on the Hilbert-Huang transform, *Mech. Syst. Signal Process.* 47 (2014) 78–93.
- [29] M. Niedzwiecki, in: *Identification of Time-Varying Processes*, Wiley, New York, 2000, p. 171.
- [30] M.D. Spiridonakos, S.D. Fassois, Non-stationary random vibration modelling and analysis via functional series time-dependent ARMA (FS-TARMA) models—A critical survey, *Mech. Syst. Signal Process.* 47 (2014) 175–224.
- [31] M. Ülker-Kaustell, R. Karoumi, Application of the continuous wavelet transform on the free vibrations of a steel-concrete composite railway bridge, *Eng. Struct.* 33 (2011) 911–919.
- [32] K. Matsuoka, K. Kaito, Hierarchical bayesian estimation of time varying vector autoregressive model, *J. Jpn Soc. Civ. Eng. Ser. A1 (Struct. Eng. Earthq. Eng. (SE/EE))* 68 (2012) 738–753 (In Japanese).
- [33] S.M. Moore, J.C.S. Lai, K. Shankar, ARMAX modal parameter identification in the presence of unmeasured excitation—I: theoretical background, *Mech. Syst. Signal Process.* 21 (2007) 1601–1615.
- [34] B.H. Kim, J. Lee, D.H. Lee, Extracting modal parameters of high-speed railway bridge using the TDD technique, *Mech. Syst. Signal Proess.* 24 (2010) 707–720.
- [35] G. Kitagawa, W. Gersch, *Smoothness Priors Analysis of Time Series*, Vol. 116, Springer Science & Business Media, 1996.
- [36] G. De Niclao, L. Magni, R. Scattolini, Stabilizing predictive control of nonlinear ARX models, *Automatica* 33 (1997) 1691–1697.
- [37] T. Arvidsson, *Train-bridge Interaction: Literature Review and Parameter Screening* PhD Thesis, KTH Royal Institute of Technology, 2014.
- [38] T. Hsiao, Time-varying system identification via maximum a posteriori estimation and its application to driver steering models. In: *American Control Conference*, 2008. IEEE, 2008, pp. 684–689.
- [39] C.M. Bishop, *Pattern Recognition and Machine Learning (Information Science and Statistics)*, Springer, New York, 2006.
- [40] L.M. Berliner, Hierarchical bayesian time series models, in: *Maximum Entropy and Bayesian Methods*, Springer, Dordrecht, 1996, pp. 15–22.
- [41] C.K. Carter, R. Kohn, On Gibbs sampling for state space models, *Biometrika* 81 (1994) 541–553.
- [42] P. De Jong, N. Shephard, The simulation smoother for time series models, *Biometrika* 82 (1995) 339–350.
- [43] J. Durbin, S.J. Koopman, A simple and efficient simulation smoother for state space time series analysis, *Biometrika* 89 (2002) 603–616.
- [44] G. Koop, D. Korobilis, Bayesian multivariate time series methods for empirical macroeconomics, *Found. Trends® in Econ.* 3 (2010) 267–358.
- [45] J. Durbin, S.J. Koopman, *Time Series Analysis by State Space Methods*, Oxford University Press, 2012.
- [46] B.D.O. Anderson, J.B. Moore, *Optimal filtering*, Englewood Cliffs, New Jersey, 1979, pp. 22–95.
- [47] C. Johansson, C. Pacoste, R. Karoumi, Closed-form solution for the mode superposition analysis of the vibration in multi-span beam bridges caused by concentrated moving loads, *Comput. Struct.* 119 (2013) 85–94.
- [48] N. Domede, A. Sellier, T. Stablon, Structural analysis of a multi-span railway masonry bridge combining in situ observations, laboratory tests and damage modelling, *Eng. Struct.* 56 (2013) 837–849.
- [49] E. Hamed, Y. Frostig, Free vibrations of cracked prestressed concrete beams, *Eng. Struct.* 26 (2004) 1611–1621.
- [50] H. Tada, P. Paris, G. Irwin, *The Analysis of Cracks Handbook* 2 (2000) 1.
- [51] S. Christides, A.D.S. Barr, One-dimensional theory of cracked Bernoulli-Euler beams, *Int. J. Mech. Sci.* 26 (1984) 639–648.
- [52] T.G. Chondros, A.D. Dimarogonas, Vibration of a cracked cantilever beam, *J. Vib. Acoust.* 120 (1998) 742–746.
- [53] M.H. Shen, Y.C. Chu, Vibrations of beams with a fatigue crack, *Comput. Struct.* 45 (1992) 79–93.
- [54] J.N. Sundermeyer, R.L. Weaver, On crack identification and characterization in a beam by nonlinear vibration analysis, *J. Acoust. Soc. Am.* 96 (1994) 3292.
- [55] M. Chati, R. Rand, S. Mukherjee, Modal analysis of a cracked beam, *J. Sound Vib.* 207 (1997) 249–270.
- [56] U. Andreaus, P. Baragatti, Experimental damage detection of cracked beams by using nonlinear characteristics of forced response, *Mech. Syst. Signal Process.* 31 (2012) 382–404.
- [57] S. Miura, H. Takai, M. Uchida, Y. Fukada, The mechanism of railway tracks, *Jpn. Rail. Transp. Rev.* 3 (1998) 38–45.
- [58] P.C. Young, Stochastic dynamic modelling and signal processing: time variable and state dependent parameter estimation, *Nonlinear Nonstationary Signal Process.* (2000) 74–114.
- [59] H. Peng, RBF-ARX model-based nonlinear system modeling and predictive control with application to a NO_x decomposition process, *Control Eng. Pract.* 12 (2004) 191–203.
- [60] A. Klepka, U.H.L. Tadeusz, Identification of modal parameters of non-stationary systems with the use of wavelet based adaptive filtering, *Mech. Syst. Signal Process.* 47 (2014) 21–34.
- [61] G. Kitagawa, W. Gersch, A smoothness priors time-varying AR coefficient modeling of nonstationary covariance time series, *IEEE Trans. Automatic Control.* 30 (1985) 48–56.
- [62] S. Frühwirth-Schnatter, Data augmentation and dynamic linear models, *J. Time Ser. Anal.* 15 (1994) 183–202.
- [63] MATLAB User's Guide. The mathworks. Inc., Natick, MA. 5 (1998) 333.
- [64] M.C. Macal, *Model Verification and Validation*, University of Chicago, 2005, pp. 1–21.
- [65] M. Sogabe, N. Matsumoto, Y. Fujino, H. Wakui, M. Kanamori, M. Miyamoto, Dynamic response and design of continuous concrete railway bridges in resonance area, *Doboku Gakkai Ronbunshu*, 2003 (2003) 83–102 (In Japanese).
- [66] A. Wiriyachai, K.H. Chu, V.K. Garg, Bridge impact due to wheel and track irregularities, *J. Eng. Mech. Division.* 108 (1982) 648–666.
- [67] Y.W. Zhang, J.H. Lin, Y. Zhao, W.P. Howson, F.W. Williams, Symplectic random vibration analysis of a vehicle moving on an infinitely long periodic track, *J. Sound Vib.* 329 (2010) 4440–4454.
- [68] X. Lei, N.A. Noda, Analyses of dynamic response of vehicle and track coupling system with random irregularity of track vertical profile, *J. Sound Vib.* 258 (2002) 147–165.
- [69] H. Takai, M. Uchida, K. Takeshita, Y. Sunaga, Track Maintenance Technique for 300 km/h class Shinkansen, 34, *Railway Technical Research Institute*, 1993, *Quarterly Reports*.
- [70] H. Tanaka, M. Matsumoto, M. Miwa, Y. Miyazaki, Comparison Analysis of Various Evaluation Indexes of Track Irregularity Data for High-speed Railway Track, *Railway Engineering-2017*, Railway Engineering, Engineering, Technics Press, Edinburgh, 2017, doi: 10.25084/raileng.2017.0021.
- [71] C. Somaschini, K. Matsuoka, A. Collina, Experimental analysis of a composite bridge under high-speed train passages, *Procedia Eng.* 199 (2017) 3071–3076.
- [72] L.F. Shampine, M.W. Reichelt, The MATLAB ode suite, *SIAM J. Sci. Comput.* 18 (1997) 1–22.